Advances in High-Resolution Spectroscopic Measurements of Molecular Ions in the Mid-Infrared

Adam J. Perry

I. INTRODUCTION

Infrared spectra of molecules typically probe transitions between rotation-vibration energy levels. Such transitions provide valuable information to theorists who try to map out the potential energy landscape of molecules and produce models and methods to predict the spectra of other molecules. Predictions of molecular vibrational spectra are becoming more commonplace, but the accuracy of such calculations is not always sufficient to the purpose. As theory marches on in hopes to be able to predict transitions with "spectroscopic accuracy," experimental data is required in order for theorists to benchmark their calculations. As the calculations become more and more accurate, so too does the need for improved experimental measurements of infrared transitions. In this prospectus the interplay between theory and experiment will be discussed as it pertains to the prediction of infrared spectra of molecular ions. The focus will come from our previous experimental work which will be described as well as proposed work to improve the measurements on a particularly important benchmark system, the H_3^+ ion. Finally, a proposed search for another theoretically interesting species, the HO_2^+ cation will be outlined.

A. Pushing the Frontiers of *ab initio* Calculations for Molecular Rovibrational Transitions

When it comes to computing rovibrational transitions of molecules with great accuracy, the interplay between experiment and theory serves as a nice example of a microcosm of science in general. First, theory makes a prediction of where in frequency space a certain transition lies, and experimentalists attempt to measure them. Once observed, the discrepancy between the experimental and the theoretical value can be used to help modify theoretical models and methodologies. As the theoretical accuracy approaches the experimental uncertainty, new and improved measurements are required to reduce the uncertainty on these frequencies. Once this has been accomplished, the theory can be revisited and further refined as the cycle continues.

Currently, it is only possible to predict rovibrational transitions to "spectroscopic accuracy" (within 1 cm^{-1}) for a select few molecular systems. The simplest of these is a single electron system, the H_2^+ ion, for which the accuracy is on the order of 10^{-5} cm^{-1}($\sim$300 kHz)

[1]. In order of increasing complexity, the next system is neutral H_2 where the accuracy of *ab initio* calculations reaches a level of $2{\times}10^{-4}$ cm^{-1}(~ 6 MHz) [2]. After H_2 the next system is HeH$^+$ which represents the simplest heteronuclear molecule. For this system the $\sim$50 measured transitions can be reproduced to roughly 0.01 cm^{-1}($\sim$300 MHz) [3]. The final major benchmark system is the simplest polyatomic molecule, the H_3^+ cation. For this species rovibrational transitions have been predicted all the way up to the dissociation limit [4] with an average accuracy on the order of 0.1 cm^{-1}. However for transitions involving low-lying rovibrational levels the accuracy is on the order of 0.01 cm^{-1}.

In order to achieve these impressive accuracies, theorists must go beyond the Born-Oppenheimer (BO) approximation. In the BO approximation the nuclei are "clamped" in place, and the electrons are assumed to relax instantaneously in response to any movement of the nuclei. This allows for the separation of the electronic and nuclear wavefunctions and as a result the electron energy becomes a parametric function of the nuclear coordinates. However, for lighter nuclei such as hydrogen and helium, this approximation begins to break down, and adiabatic and nonadiabatic corrections need to be introduced. Also, when the desired accuracy is on the order of fractions of a wavenumber, effects arising from relativity and quantum electrodynamics (QED) need to be considered as well, which is where much of the current research focuses.

The typical approach is to generate a BO potential energy surface, then produce surfaces for each type of correction accounted for. The final potential energy surface is simply the sum of the BO surface and all the correction surfaces, and it is from this surface that rovibrational transitions are computed. This is also where improved experimental measurements of rovibrational transitions become useful. As the quality of the measurements increases (i.e. a reduction in the measurement uncertainty) they serve as better benchmark values to which the computed transitions can be compared. This allows theorists to refine their methodologies for computing the various correction surfaces and improve the accuracy of their calculations.

B.   Instrument Description

With the advent of velocity modulation spectroscopy (VMS) in 1983 by Richard Saykally [5], the field of molecular ion spectroscopy greatly expanded. In this technique ions of

interest are produced in an AC positive column discharge. As a result of the rapidly changing polarity of the electrodes, the ions' velocities are modulated at the frequency at which the plasma is driven, which also periodically Doppler shifts the ions' absorption profiles on and off resonance with the probing laser beam. By measuring the transmitted light through lock-in detection it is possible to recover only the signals from ions and reject the much more dominant neutral signals. This technique has been the workhorse of the field for many years; however, it is possible to improve the sensitivity of this technique. By surrounding the discharge with a pair of highly reflective mirrors, we can increase the number of passes the laser makes through the discharge and hence increase the signal strength. It is also possible to drastically reduce technical noise in the spectra by encoding the signal at a high frequency (typically a radio frequency) through the use of heterodyne detection. These three methods can be combined into a single technique called Noise Immune Cavity Enhanced Optical Heterodyne Velocity Modulation Spectroscopy (NICE-OHVMS). Demonstration of this technique was initially performed by Siller et al. [6].

The instrument described here is the first implementation of NICE-OHVMS in the mid-infrared, and a detailed description of it can be found in the attached paper by Crabtree et al. [7]. In short, the instrument (Figure 1) uses a high power (~1 W), mid-infrared continuous wave optical parametric oscillator (OPO) as the light source. The OPO is pumped by an ytterbium-doped fiber laser operating at 1064 nm which is phase modulated by an electro-optic modulator to produce sets of RF sidebands for heterodyne spectroscopy (~80 MHz) and Pound-Drever Hall locking (~2 MHz). The modulated pump light is then amplified to a power of ~10 W with a fiber amplifier. Pump radiation is then fiber coupled into a bow-tie cavity containing a periodically-poled lithium niobate crystal, where optical parametric oscillation occurs. Pump photons are split into signal photons (1.5 - 1.6 μm) which are resonant with the cavity, and idler photons (3.2 - 3.9 μm) which are used to perform spectroscopy. The sidebands are imprinted on the idler during this process.

The idler beam is then coupled into an external optical cavity which surrounds a specially designed positive column discharge cell named Black Widow (Figure 2). Inside the cell a mixture of precursor gasses is struck by an AC (~40 kHz) discharge to form a plasma, which is where ion production occurs. Due to the enhanced intracavity power as well as the bidirectional nature of the cavity, sub-Doppler spectroscopy is possible. The sub-Doppler features, or Lamb dips, are typically an order of magnitude narrower than the Doppler

3

profile, which enhances both the resolution of the instrument and the precision to which line centers can be fit.

The light transmitted through the cavity is used for heterodyne detection where the resulting signal is demodulated at the heterodyne frequency of $\sim$80 MHz by two mixers set to be 90 degrees out of phase with one another. The mixer outputs are then demodulated again using a pair of lock-in amplifiers referenced to twice the AC discharge frequency for recovery of the velocity modulation information.

Frequency calibration is accomplished using either a commercial near-infrared wavemeter, which is only accurate to within $\sim$70 MHz, or an optical frequency comb. It is the frequency comb which allows for very precise frequency calibration which in turn enables us to measure transition frequencies with sub-MHz precision. The idler frequency is determined by measuring difference between the pump and signal beam frequencies.

II. COMPLETED WORK

A. Sub-MHz Precision Measurements of Rovibrational Transitions of HCO^+

Demonstration of our ability to measure infrared transitions of molecular ions with sub-MHz precision was carried out using the well-studied ion HCO^+ as a test case [8]. Unfortunately, it was discovered that the high reflectivity mirrors comprising the external optical cavity were defective, thus making it impossible to perform NICE-OHVMS. Therefore, the cavity mirrors were removed, and single-pass optical heterodyne velocity modulation spectroscopy was performed instead. These measurements marked the first comb-calibrated spectra recorded on this instrument. Despite the inability to use cavity enhancement, strong Doppler-broadened signals were observed arising from 20 rovibrational transitions in the ν_1 fundamental band with signal-to-noise ratios of $\sim$300 for the strongest lines and $\sim$100 for the weakest lines. Many of the 20 lines measured were done so with sub-MHz precision with the average statistical uncertainty being 600 kHz. All transitions from P(10) to R(9) were measured and were fit to the second derivative of a Gaussian function in order to approximate the two layers of modulation provided by the heterodyne detection and the velocity modulation of the ions.

In order to confirm the accuracy of our measurements, a combination difference analysis

was performed in which rotational energy level spacings were determined from the rovibrational transitions (Figure 3). Using the previously measured values for the J = 1 ← 0 transition in the ground vibrational state [9] and the J = 3 ← 2 transition in the $1\nu_1$ vibrationally excited state [10], spacings between adjacent rotational levels can be inferred. This yielded pure rotational transitions that can be compared to direct laboratory measurements. The results of this analysis can be found in Siller *et al.* which is also attached [8]. It was found that all calculated rotational transitions agreed to within 2.8 MHz of directly observed transitions in the ground vibrational state and within 5.0 MHz of previously measured transitions in the $1\nu_1$ state, which suggests a high degree of accuracy in our measurements.

As a second check of our frequencies, the rovibrational transitions were fit to an effective Hamiltonian of a linear molecule to determine the associated spectroscopic constants and to compare them to previously determined values. Comparison of the ground state constants (B and D) show excellent agreement with those reported by Cazzoli et al. [9] while those of the excited state (the band origin, B, and D constants) all agree to within 1σ of those determined by Hirao et al. [11]

B.   NICE-OHVMS with Frequency Comb Calibration

After acquiring a new set of mirrors for the cavity, we were able to return to performing NICE-OHVMS, this time with frequency comb calibration. As a first target for testing out the full capabilities of the spectrometer, sub-Doppler spectra of H_3^+ were recorded. At this time ten rovibrational transitions in the ν_2 fundamental band were recorded with eight out of the ten lines measured with sub-MHz precision (the statistical precision limited by the signal-to-noise on some transitions).

The first sub-Doppler spectrum of H_3^+ was acquired by the group of J.T. Shy and was recorded for the R(1,0) transition in the ν_2 fundamental band using a strong pump weak probe technique [12]. Comparison of our measured line center for this transition to that of Shy's group yields a ∼5 MHz discrepancy. Given that their claimed uncertainty was ∼250 kHz and ours was 230 kHz this was a major concern. Comparison to other transition frequencies measured in Shy's lab (the $R(1,1)^l$ and $R(1,1)^u$ transitions [13]) also yielded discrepancies that were on the order of 10 MHz but of random sign. As a result we went to great lengths to evaluate any sources of error in our experiment. Effects such as signal-to-

noise ratio, asymmetry in the obtained line shapes, pressure shifts, and functionality of the frequency comb were carefully examined. The details of this analysis can be found in the attached paper by Hodges *et al.* [14]. None of the examined effects were found to account for the discrepancy between the two sets of measurements.

To assess the accuracy of our measurements, we revisited HCO^+ with sub-Doppler spectroscopy. Two transitions, the P(5) and R(3) lines, were re-measured with 500 kHz and 400 kHz statistical uncertainty respectively. Subtracting these two frequencies yields a combination difference corresponding to the energy spacing between the J = 3 and J = 5 levels in the ground vibrational state. This spacing matched the sum of the J = 4 ← 3 and J = 5 ← 4 rotational transitions that were measured by Cazzoli *et al.* [9] to within 500 kHz. The good agreement between the rotational work and our measurements was encouraging to us and lends credibility to the accuracy of our measurements.

A second independent confirmation of our ability to accurately measure line centers came from a measurement of a rovibrational transition of the CH_5^+ ion. This particular transition was also recoded by the Oka group in 1999 [15], and also marks the first ever sub-Doppler spectrum of CH_5^+. Figure 4 shows the average of five comb-calibrated scans of the transition reported by Oka at 2898.008 cm^{-1}. A fit of the central Lamb dip yields a transition frequency of 86 880 178.469(126) MHz. The Schlemmer group in Cologne has also measured this CH_5^+ transition to be 86 880 178.22(63) MHz [16], which is only ∼240 kHz different from our measurement [14]. The difference between the two measurements is well within 1σ of the uncertainty claimed by Schlemmer, which further enhanced the confidence we have in our accuracy.

C.   High-Precision Spectroscopic Measurements of the HeH^+ Cation

With confirmation of our ability to accurately measure transition line centers, the next undertaking was a high-precision spectroscopic survey of HeH^+. This ion is one of the important benchmark systems for *ab initio* calculations as it is the simplest heteronuclear molecule (and is also isoelectronic to H_2). The state-of-the art *ab initio* calculations performed on this molecule which take into account the adiabatic, nonadiabatic, relativistic, and leading QED corrections to the Born-Oppenheimer approximation are able to reproduce many of the experimentally measured rovibrational transition frequencies to within 0.01 cm^{-1}[3]. This

level of accuracy is only two to five times larger than the previously reported experimental uncertainty (0.002-0.005 cm^{-1}), which means that improved measurements are expected to be needed in the near future in order to allow for the advancement of theoretical treatments of this molecule.

Using our NICE-OHVMS spectrometer I was able to re-measure seven rovibrational transitions of HeH$^+$ in the fundamental vibrational band. The measured transitions included the P(3)-R(3) lines and were mostly measured with sub-MHz precision, an improvement in the experimental uncertainty of nearly two orders of magnitude over the previous measurements of Bernath and Amano [17]. All results from these measurements can be found in the attached paper by Perry *et al.* From these data, a new set of experimentally determined rovibrational levels for HeH$^+$ can be constructed in which eight of the levels are determined with MHz or sub-MHz precision. The new values for these energy levels should provide theorists with new and improved "targets" to which new theoretical predictions of the rovibrational levels of HeH$^+$ can be benchmarked, paving the way for treatments of the remaining nonadiabatic, relativistic, and QED contributions to the potential energy surface.

III. PROPOSED WORK

A. High-Precision Spectroscopic Survey of H$_3^+$

The accuracy of theoretically predicted rovibrational transitions of H$_3^+$ ($\sim$0.01 cm^{-1}or even better in some cases) is essentially at the level of the current experimental precision of laboratory measurements (0.002-0.01 cm^{-1}) [18] (with the exception of the handful of measurements made by Wu *et al.* [19] and in our lab [14]). This means that a large high-precision survey of this molecule is needed.

Experimentally, this work will be an extension of the measurements demonstrated earlier, where the plan is to first measure as many fundamental band transitions as we can. Based on the current sensitivity of the instrument, which is 1.5×10^{-9} cm^{-1}Hz$^{-1/2}$, and its frequency coverage (2564-4000 cm^{-1}), it should be possible to re-measure $\sim$200 fundamental band transitions with MHz or sub-MHz precision. From these measurements the spacing between rovibrational levels within a given "G stack" can be determined. Once this is accomplished, transitions in the $2\nu_2^2 \leftarrow 1\nu_2^1$ hot band will be measured in order to probe rotational levels in

the $2\nu_2^2$ state. After measurement of the hot band transitions it is possible to link different G stacks together through the $2\nu_2^2 \leftarrow 0$ overtone transitions (which have the selection rule $\Delta G = 3$). Figure 5 illustrates this combination difference scheme.

After all the measurements have been completed and the G stacks have been tied together, it will be necessary to tie the *ortho*-H_3^+ (G = 3n) and *para*-H_3^+ (G = 3n±1) stacks together. This can be accomplished through a global fit of all determined energy levels to the energy level expression given in Lindsay and McCall [18]. Performing this sort of analysis will yield an accurate list of rovibrational energy levels for H_3^+ in which the experimental uncertainty is on the order of 1 MHz or better. These improved levels will serve as excellent benchmark values as theory looks to improve upon the treatment of nonadiabatic and QED effects to the potential energy surface of this molecule.

B. Discovery Spectroscopy of Protonated Oxygen HO_2^+

To date, nearly all the protonated diatomics have been studied spectroscopically with high resolution. One such species that has eluded such studies for roughly 30 years is protonated oxygen, HO_2^+. Most of the previous work performed on this molecule involves theoretical predictions for the band centers for the three fundamental modes. The first prediction of the ν_1 band origin was carried out by Dyke and coworkers who used photoelectron spectroscopy to measure the first ionization potential of neutral HO_2 [20]. Using force constants derived previously by Van Lenthe and Ruttnik they predicted the ν_1 band to be at 3577 cm^{-1}[20, 21].

After this initial prediction, the HO_2^+ ion was the subject of many more theoretical investigations [22–24]. As a result, the prediction of the ν_1 band origin trended to lower frequency where the predictions of Quelch *et al.* yielded a band origin of 3140 cm^{-1}[22]. Despite all of these theoretical efforts to assist laboratory detection of HO_2^+, no detection in the mid-infrared was made. However, an extensive search for the high-resolution spectrum was carried out by the Oka group in 1991 [25].

In 1997, Nizkorodov *et al.* revisited the problem by performing photodissociation spectroscopy of He and Ne tagged HO_2^+ molecules [26]. Though they were not able to measure the ν_1 frequency directly (of bare HO_2^+), they were able to put an estimate on the band origin of 3020 ± 40 cm^{-1}, which was much lower than any previous theoretical calculation. This spurred more theoretical work on the molecule and it was not until 2008 when Huang and

Lee [27] performed coupled cluster calculations that yielded a prediction of 3022 cm^{-1} that agreed well with the estimation given by Nizkorodov. Huang and Lee's calculation was followed up by another study by Widicus Weaver *et al.* who used a larger basis set and treated spin-orbit as well as spin-rotation couplings [28]. Their prediction of the ν_1 frequency (3028 cm^{-1}) also falls within the estimation of Nizkorodov. The most recent detection of HO$_2^+$ was made by Jacox *et al.* and was done in a solid helium matrix using FTIR spectroscopy [29]. However, in this study the ν_1 band was not observed and only evidence for the ν_2 bending mode at 1026.5 cm^{-1} was established.

Based on the previous work involving this molecule, a new search using the NICE-OHVMS technique seems to be the next step in trying to observe the high-resolution infrared spectrum of HO$_2^+$. In order to do this, wide frequency scans will be performed which are centered about the ~3020 cm^{-1} band center that was estimated by Nizkorodov [26] and supported theoretically by the works of Huang and Lee [27] and Widicus Weaver *et al.* [28].

To get a sense for the expected number density of HO$_2^+$ produced in our experiment, one can examine its primary formation mechanism:

$$H_3^+ + O_2 \rightleftharpoons HO_2^+ + H_2 \tag{1}$$

Using the expression for the equilibrium constant of this reaction, the following estimation for the number density of HO$_2^+$ can be made:

$$[HO_2^+] = K(T)\frac{[H_3^+][O_2]}{[H_2]} \tag{2}$$

Here K(T) is the equilibrium constant for reaction (1) as a function of temperature. The value taken from Widicus Weaver *et al.* is defined for a temperature of 300 K where K(T)=2.025 [28]. Given that the temperature of a water-cooled discharge is likely to be greater than 300 K, this value of K(T) is likely underestimated because of the slight endothermicity of reaction (2) [28]. Therefore, this value provides a lower bound on the predicted number density of HO$_2^+$. Estimates for the number density of H$_3^+$ can be made using the work of Cordonnier *et al.* [30], which, for 1 torr of H$_2$ should yield $[H_3^+] \approx 1 \times 10^{10}$ cm^{-3}. If a 1:1 mixture of H$_2$:O$_2$ is used, it can be estimated from Equation 2 that the HO$_2^+$ number density is 2×10^{10} cm^{-3}.

To get a sense for the number of observable lines in the spectrum, the ν_1 band was simulated using PGopher [31]. Figure 6 shows the simulated spectrum. The spectrum was

generated using the calculated spectroscopic constants found in reference [28] and assumes a molecule with C_s symmetry. The difference in the ground and excited state parameters was approximated by determining the fractional change of those measured for neutral HO_2 [32]. The same fractional change was then applied to the calculated ground state spectroscopic constants. Based on this simulation and the calculated integrated band intensity of 544 km/mol [22], at least 200 lines should be observable with a signal-to-noise ratio greater than six. With this many observable lines, it should at least be possible to measure many spectroscopic parameters of the molecule which should yield an interesting comparison to all the theoretical work that has been published on this molecule.

IV. SUMMARY

Demonstrations of the capabilities of the first mid-infrared NICE-OHVMS spectrometer have been presented through high-precision measurements of HCO^+, H_3^+, CH_5^+, and HeH^+. The ability to measure rovibrational transitions of molecular ions to MHz or sub-MHz precision will allow for advancements to be made in theoretical predictions of the rovibrational spectra of molecules. These measurements of the transition frequencies will likely serve as lasting benchmarks for years to come. Not only is this instrument capable of high-precision spectroscopy, but its sensitivity should allow for the detection of species that have eluded experimentalists for years, most notably the HO_2^+ ion.

[1] V. Korobov, "Relativistic corrections of mα^6 order to the rovibrational spectrum of H_2^+ and HD^+ molecular ions" *Phys. Rev. A* (2008), **77**(2), 022509.

[2] G. D. Dickenson, M. L. Niu, E. J. Salumbides, J. Komasa, K. S. E. Eikema, K. Pachucki, W. Ubachs, "Fundamental vibration of molecular hydrogen" *Phys. Rev. Lett.* (2013), **110**(19), 193601.

[3] K. Pachucki, J. Komasa, "Rovibrational levels of helium hydride ion." *J. Chem. Phys.* (2012), **137**(20), 204314.

[4] M. Pavanello, L. Adamowicz, A. Alijah, N. F. Zobov, I. I. Mizus, O. L. Polyansky, J. Tennyson, T. Szidarovszky, A. G. Császár, "Calibration-quality adiabatic potential energy surfaces for

H$_3^+$ and its isotopologues." *J. Chem. Phys.* (2012), **136**(18), 184303.

[5] C. S. Gudeman, M. H. Begemann, J. Pfaff, R. J. Saykally, "Velocity-modulated infrared laser spectroscopy of molecular ions: The ν_1 band of HCO$^+$" *Phys. Rev. Lett.* (1983), **50**(10), 727–731.

[6] B. M. Siller, M. W. Porambo, A. A. Mills, B. J. McCall, "Noise immune cavity enhanced optical heterodyne velocity modulation spectroscopy." *Opt. Express* (2011), **19**(24), 24822–7.

[7] K. N. Crabtree, J. N. Hodges, B. M. Siller, A. J. Perry, J. E. Kelly, P. A. Jenkins, B. J. McCall, "Sub-Doppler mid-infrared spectroscopy of molecular ions" *Chem. Phys. Lett.* (2012), **551**, 1–6.

[8] B. M. Siller, J. N. Hodges, A. J. Perry, B. J. McCall, "Indirect Rotational Spectroscopy of HCO$^+$" *J. Phys. Chem. A* (2013).

[9] G. Cazzoli, L. Cludi, G. Buffa, C. Puzzarini, "Precise THz measurements of HCO$^+$, N$_2$H$^+$, and CF$^+$ for astronomical observations" *Astrophys. J. Suppl. Ser.* (2012), **203**(1), 11.

[10] V. Lattanzi, A. Walters, B. J. Drouin, J. C. Pearson, "Rotational spectrum of the formyl cation, HCO$^+$, to 1.2 THz" (2007), (1981).

[11] T. Hirao, S. Yu, T. Amano, "Submillimeter-wave spectroscopy of HCO$^+$ in the excited vibrational states" *J. Mol. Spectrosc.* (2008), **248**(1), 26–40.

[12] H.-C. Chen, C.-Y. Hsiao, J.-L. Peng, T. Amano, J.-T. Shy, "High-Resolution sub-Doppler lamb dips of the ν_2 fundamental band of H$_3^+$" *Phys. Rev. Lett.* (2012), **109**(26), 263002.

[13] J.-T. Shy, private communication (2013).

[14] J. N. Hodges, A. J. Perry, P. A. Jenkins, B. M. Siller, B. J. McCall, "High-precision and high-accuracy rovibrational spectroscopy of molecular ions" *J. Chem. Phys.* (2013), **139**(16), 164201.

[15] E. T. White, "CH$_5^+$: The infrared spectrum observed" *Science* (1999), **284**(5411), 135–137.

[16] S. Schlemmer, private communication (2013).

[17] P. Bernath, T. Amano, "Detection of the infrared fundamental band of HeH$^+$" *Phys. Rev. Lett.* (1982), **48**(1), 20–22.

[18] C. Lindsay, B. J. McCall, "Comprehensive evaluation and compilation of H$_3^+$ spectroscopy" *J. Mol. Spectrosc.* (2001), **210**, 60–83.

[19] K.-Y. Wu, Y.-H. Lien, C.-C. Liao, Y.-R. Lin, J.-T. Shy, "Measurement of the ν_2 fundamental band of H$_3^+$" *Phys. Rev. A* (2013), **88**(3), 032507.

[20] J. Dyke, N. Jonathan, A. Morris, M. Winter, "Vacuum ultraviolet photoelectron spectroscopy of transient species" *Mol. Phys.* (1981), **44**(5), 1059–1066.

[21] J. H. Van Lenthe, P. J.A. Ruttink, "Ab initio calculations on the three lowest states of HO_2^+" *Chem. Phys. Lett.* (1978), **56**(1), 20–24.

[22] G. E. Quelch, Y. Xie, B. F. Yates, Y. Yamaguchi, H. F. Schaefer, "The HO_2^+ ion" *Mol. Phys.* (1989), **68**(5), 1095–1109.

[23] D. J. DeFrees, A. D. McLean, "Molecular orbital predictions of the vibrational frequencies of some molecular ions" *J. Chem. Phys.* (1985), **82**(1), 333.

[24] G. P. Raine, H. F. Schaefer, N. C. Handy, "The HO_2^+ molecular ion. Geometrical structure and vibrational frequencies" *J. Chem. Phys.* (1984), **80**(1), 319.

[25] W. Ho, C. Pursell, T. Oka, "Infrared spectroscopy in an H_2-O_2-He discharge: H_3O^+" *J. Mol. Spectrosc.* (1991), **149**(2), 530–541.

[26] S. A. Nizkorodov, D. Roth, R. V. Olkhov, J. P. Maier, O. Dopfer, "Infrared predissociation spectra of He-HO_2^+ and Ne-HO_2^+: prediction of the ν_1 frequency of HO_2^+" *Chem. Phys. Lett.* (1997), **278**(1), 26–30.

[27] X. Huang, T. J. Lee, "A procedure for computing accurate ab initio quartic force fields: Application to HO_2^+ and H_2O." *J. Chem. Phys.* (2008), **129**(4), 044312.

[28] S. L. Widicus Weaver, D. E. Woon, B. Ruscic, B. J. McCall, "Is HO_2^+ a detectable interstellar molecule?" *Astrophys. J.* (2009), **6971-s2.0-**(1), 601–609.

[29] M. E. Jacox, W. E. Thompson, "Infrared spectra of products of the reaction of H atoms with O_2 trapped in solid neon: HO_2, HO_2^+, $HOHOH^-$, and $H_2O(HO)$." *J. Phys. Chem. A* (2012), **117**(39), 9380–9390.

[30] M. Cordonnier, D. Uy, R. M. Dickson, K. E. Kerr, Y. Zhang, T. Oka, "Selection rules for nuclear spin modifications in ion-neutral reactions involving H_3^+" *J. Chem. Phys.* (2000), **113**(8), 3181.

[31] C. Western, "PGOPHER, a Program for Simulating Rotational Structure" (2009).

[32] C. Yamada, "Difference frequency laser spectroscopy of the ν_1 band of the HO_2 radical" *J. Chem. Phys.* (1983), **78**(7), 4379.
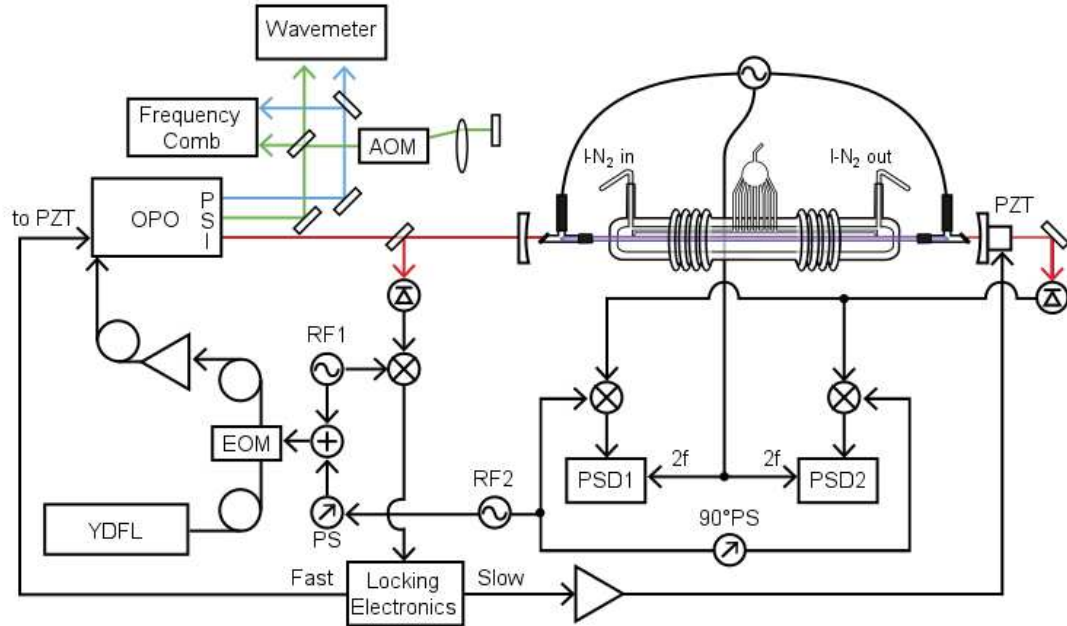
Figures

FIG. 1: A block diagram of the NICE-OHVMS Spectrometer. (YDFL: Ytterbium Doped Fiber Laser, EOM: Electro-optic Modulator, OPO: Optical Parametric Oscillator, P: Pump, S: Signal, I: Idler, PZT: Piezo Transducer, PSD: Phase Sensitive Detector, RF: Radio Frequency Generator, PS: Phase Shifter, AOM: Acousto-optic Modulator)
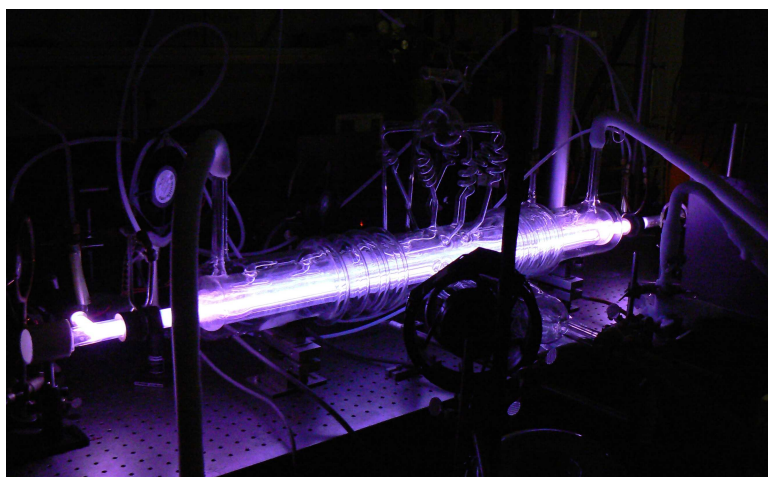
FIG. 2: A photograph of the positive column named discharge cell named Black Widow which is used to produce ions. The velocity of the ions is modulated by striking an AC discharge across a mixture of precursor gasses.
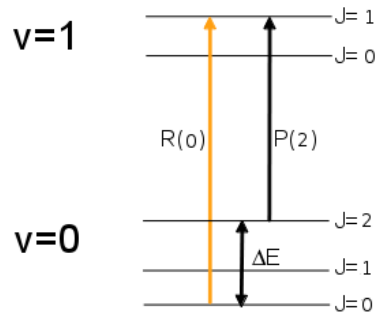
FIG. 3: Illustration of how a combination difference of rovibrational transitions yields rotational energy level spacings. In this particular case the difference between the R(0) and P(2) transitions yields the spacing between the J = 0 and J = 2 levels in the ground vibrational state.
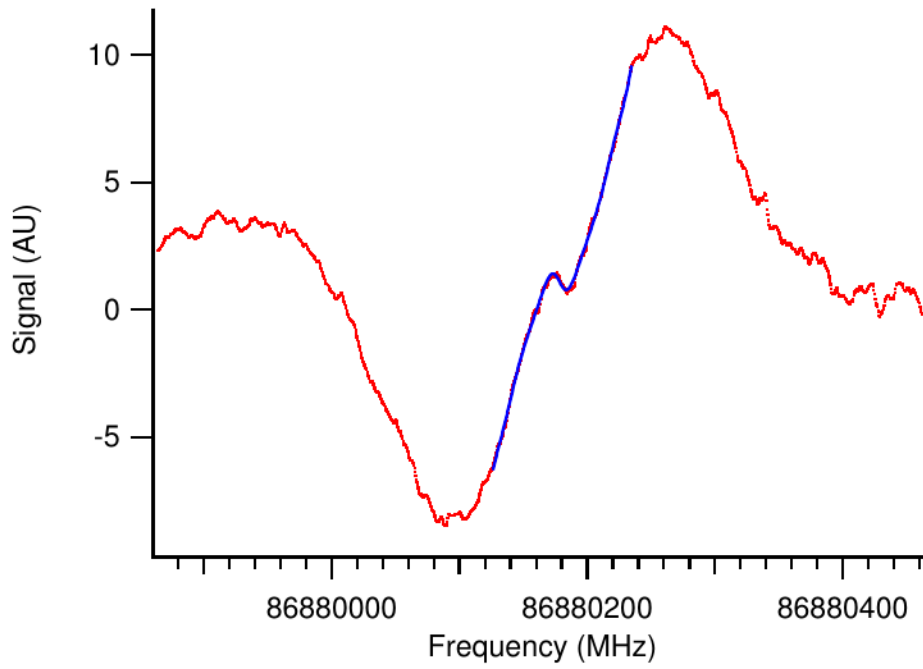
FIG. 4: Scan of the first sub-Doppler spectrum of the CH_5^+ molecular ion. The trace (black) represents the average of five scans. A fit (blue) of the central Lamb dip feature yields a line center of 86880178.469(126) MHz (Ref. [14]) which compares very well to the measurement of the Schlemmer group (86880178.22(63) MHz).
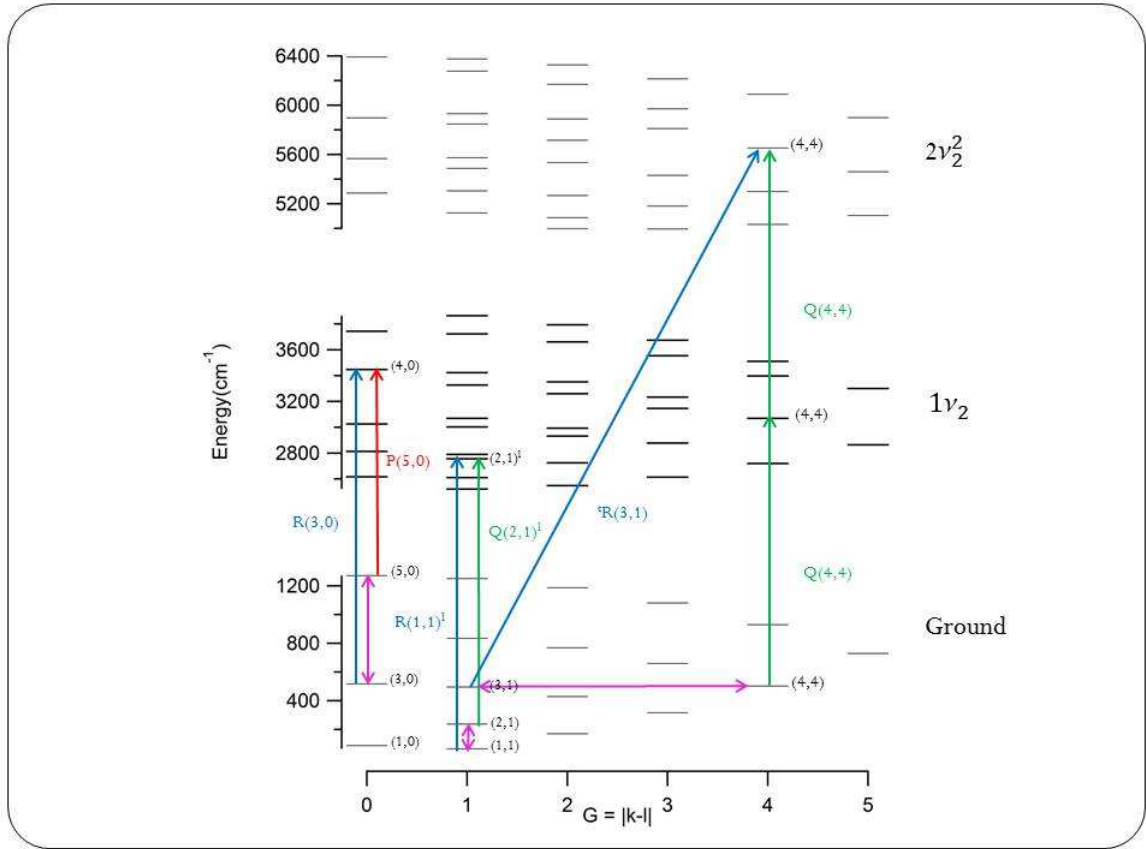
16

FIG. 5: Combination difference scheme to experimentally determine rovibrational levels of H_3^+. For $G \neq 0$ pairs of Q and R branch transitions sharing a common level will yield adjacent rotational level spacings. For the case when $G = 0$ pairs of P and R branch transitions will be needed as levels with even J are symmetry forbidden in the ground state. In order to tie different G ladders together, a three-line combination difference consisting of a fundamental, hot band, and overtone transition (which have the selection rule $\Delta G = 3$) can be employed.
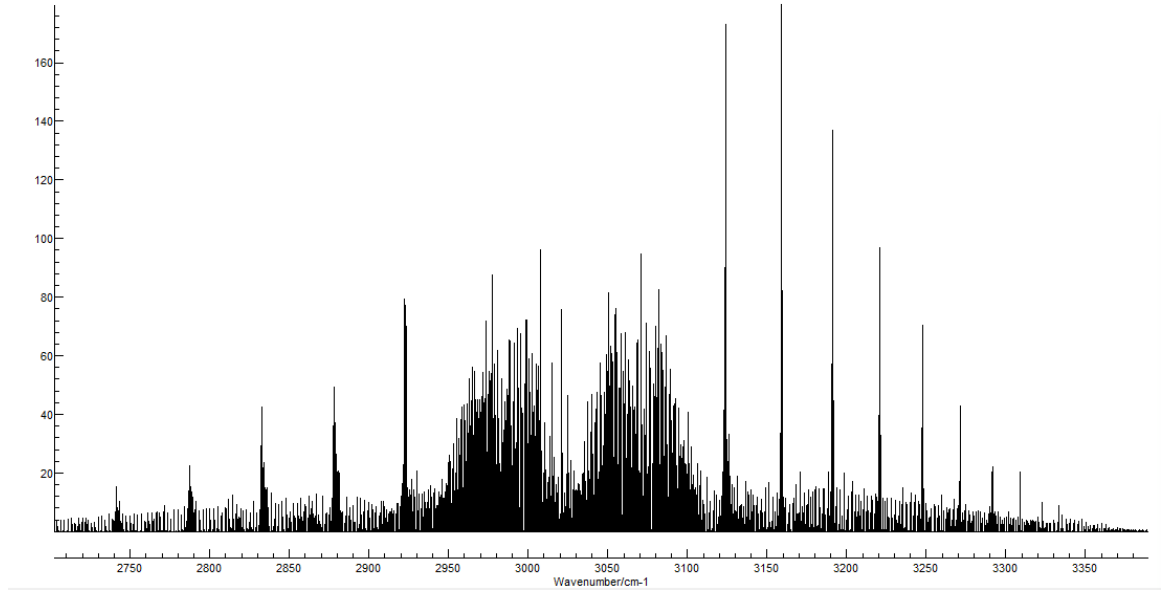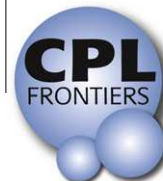
17

FIG. 6: Simulation of the ν_1 fundamental band of HO_2^+. The simulation uses the calculated ground state spectroscopic constants of Ref.[28]. Upper state constants were estimated by applying the fractional change in the ground state constants observed in neutral HO_2 (Ref.[32])

FRONTIERS ARTICLE

Sub-Doppler mid-infrared spectroscopy of molecular ions

Kyle N. Crabtree [a,1], James N. Hodges [a], Brian M. Siller [a], Adam J. Perry [a], Joseph E. Kelly [a],
Paul A. Jenkins II [a], Benjamin J. McCall [a,b,*]

[a] Department of Chemistry, University of Illinois, Urbana, IL 61801, USA
[b] Departments of Astronomy and Physics, University of Illinois, Urbana, IL 61801, USA

ARTICLE INFO

ABSTRACT

The technique of velocity modulation spectroscopy has recently been combined with cavity enhancement and frequency modulation methods into a technique called noise-immune cavity-enhanced optical heterodyne velocity modulation spectroscopy (NICE-OHVMS). We have implemented NICE-OHVMS with a cw-optical parametric oscillator (OPO) tunable from 3.2 to 3.9 μm, and used it to record spectra of the $R(1,0)$ and $R(1,1)^u$ transitions of the v_2 fundamental band of H_3^+. The high optical power and cavity enhancement enable saturation of rovibrational transitions, which allows for line center frequencies to be measured with a precision of 70 kHz.

© 2012 Elsevier B.V. All rights reserved.

1. Introduction

Molecular ions play a key role as intermediates in chemical reactions, and a detailed understanding of their structure and intramolecular dynamics in the gas phase, generally obtained by spectroscopy, is a critical first step toward understanding their behavior in more complicated systems. The primary technique used for ion spectroscopy over the past 30 years has been velocity modulation spectroscopy (VMS) [1,2]. In VMS, ions are produced in an AC positive column plasma whose polarity is alternated at frequency f_{vm}. The average drift velocity of the ions in the plasma is shifted toward the cathode from the applied electric field, while neutral molecules are generally unaffected. As the polarity is reversed, the average ion drift velocity also reverses, resulting in a periodic oscillation in the ion velocity distribution at f_{vm}. By interrogating the ions with a laser beam passing in one direction through the plasma, the absorption profiles are alternately red- and blue-shifted with respect to their rest frequencies, and phase-sensitive detection at f_{vm} allows for selective retrieval of ionic signals. VMS therefore addresses one of the main challenges of ion spectroscopy, i.e., detection of ionic species that are only $\sim 10^{-5} - 10^{-6}$ as abundant as neutral molecules. Well over 40 unique molecular ions (not including isotopologues) have been de-

tected with VMS; these have been extensively reviewed by Stephenson and Saykally [3].

Recently, the use of a Fabry–Perot optical cavity to enhance the optical path length was demonstrated by Siller et al. (cavity-enhanced velocity modulation spectroscopy, CEVMS), who locked a Ti:Sapphire laser to an optical cavity surrounding a velocity modulated positive column cell and detected the transmitted light [4]. Because the light in the cavity is bidirectional, red and blue Doppler shifts are simultaneously superimposed, encoding the velocity modulation (VM) signal at $2f_{vm}$. Initially, this was believed to be problematic because any neutral molecules produced or excited by the discharge are concentration modulated (CM) at $2f_{vm}$; that is, the population of the excited species varies with the magnitude of the applied voltage, but not the sign of the voltage. By also encoding the ion signal at $2f_{vm}$, it was thought the concentration modulation signal of neutral molecules would overwhelm the ion velocity modulation signal. Siller et al. showed that the ion and neutral signals occurred at different phases with respect to the plasma voltage, thereby preserving ion-neutral discrimination through phase-sensitive detection. Additionally, the power enhancement from the optical cavity enables saturation spectroscopy and precise line-center determination [5]. A related technique has also been employed using an optical frequency comb as the light source and a unidirectional ring cavity surrounding a plasma cell, effectively converting VMS to a broadband technique while preserving the high resolution of laser spectroscopy [6].

Cavity enhanced absorption spectroscopy suffers from the fact that frequency noise in the laser is directly converted into intensity noise as a result of reduced cavity transmission. This limitation was overcome by Ye et al. with noise-immune cavity-enhanced

optical heterodyne molecular spectroscopy (NICE-OHMS) [7]. In this technique, the laser is phase modulated at f_h (typically ~100s of MHz), effectively generating an FM triplet consisting of a carrier (at the optical frequency f_o) and a pair of sidebands with opposite phase at $f_o \pm f_h$. The triplet is coupled into the optical cavity by setting f_h equal to an integer multiple of the cavity free spectral range (FSR). In the absence of any intracavity absorption or dispersion, the beat notes between each sideband beating with the carrier are balanced in both amplitude and phase, so there is no net signal at f_h. However, in the presence of an intracavity absorber or disperser, the beat notes are unbalanced in amplitude and/or phase, yielding a net signal. By encoding absorption/dispersion information at a high frequency, $1/f$ technical noise is reduced. Another advantage is that any laser frequency noise affects the cavity coupling efficiency of the carrier and both sidebands equally, which keeps the beat notes of each sideband with the carrier balanced, and eliminates direct conversion of laser frequency noise to noise in the final spectrum. The disadvantages are the complexity of the technique, particularly the demands of maintaining the laser-cavity lock, and the requirement of a detector whose bandwidth is at least f_h. An extensive review of the NICE-OHMS technique has been published by Foltynowicz et al. [8].

CEVMS and NICE-OHMS have been combined into a technique called noise-immune cavity enhanced optical heterodyne velocity modulation spectroscopy (NICE-OHVMS) in the near-infrared with a Ti:Sapphire laser [9]. Because f_h and f_{vm} are at significantly different frequencies (typically ~100 MHz and ~10 kHz, respectively), the detector signal is first demodulated at f_h, and then sent on to further phase-sensitive detection at $2f_{vm}$. NICE-OHVMS preserves the ion-neutral discrimination afforded by VMS, and takes advantage of the ultra-high sensitivity, saturation, and noise immunity of NICE-OHMS.

However, the technical demands of the NICE-OHMS technique have largely precluded its use in the mid-infrared spectral region in which VMS has been successfully exploited. The high bandwidth detectors and phase modulators required for NICE-OHMS are not as readily available in the mid-IR compared with the visible/near-IR. The only published mid-IR NICE-OHMS work was done with a quantum cascade laser near 8.5 μm, and was limited by the detector bandwidth and the phase modulation characteristics of the device [10]. Work is currently underway in our laboratory to extend NICE-OHMS into the mid-IR using a difference frequency generation (DFG) source in the 3–5 μm region [11], which is particularly attractive for a general-purpose ion spectrometer because the vast majority of molecules have at least one fundamental vibrational band in that portion of the spectrum.

Here we report the first mid-IR NICE-OHVMS spectrometer, which uses a commercially available cw-optical parametric oscillator (OPO) tunable from 3.2 to 3.9 μm. The high optical power of the OPO (~1 W) allows for use of high bandwidth mid-IR detectors that are not sensitive enough to be used with many other lower-power cw lasers in this region. This technique enables all of the advantages of the NICE-OHVMS technique to be brought to bear on fundamental vibrational transitions of molecular ions, including high precision sub-Doppler spectroscopy.

Our initial demonstration of this instrument focuses on the study of H_3^+, which is the simplest polyatomic molecular ion and serves as the primary initiator of ion–molecule chemistry in interstellar clouds [12,13]. Its infrared spectrum was first observed by Oka in 1980 [14], and since then it has been extensively studied spectroscopically (see, for instance, the review in Ref. [15]). More recent research on H_3^+ focuses on spectroscopy above the so-called "barrier to linearity," at which point the molecule adopts a linear geometry that induces a singularity in the Hamiltonian, complicating its theoretical treatment [16]. Nevertheless, for the lowest-lying energy levels, the agreement between experiment and ab

initio theory is good to spectroscopic accuracy [17]. Measuring the energy level spacings experimentally with higher precision and accuracy would present a greater challenge for ab initio theory, possibly spurring new developments. The NICE-OHVMS technique opens the possibility of measuring such energy level spacings in H_3^+.

As a demonstration of the capabilities of this instrument, we present in this Letter spectra of the v_2 fundamental band of H_3^+ at 3.67 μm. In Section 2 we describe the instrumental details, and in Section 3 we discuss NICE-OHVMS lineshapes and present spectra acquired with the instrument. Finally, in Section 4, the performance of the instrument is assessed, and future directions are discussed.

2. Experimental details

Our NICE-OHVMS instrument is outlined in Figure 1. A Ytterbium-doped fiber laser (YDFL, Koheras Adjustik Y-10) is sent through a fiber EOM (EOSPACE PM-0K5–00-PFU-PFU-106-S), amplified (IPG Photonics YAR-10 K-1064-LP-SF), and used to pump a singly-resonant OPO (Aculight Argos 2400 SF). The pump (1.064 μm) and signal (1.5–1.6 μm) beams are sent to a wavemeter (Burleigh WA-1500) for frequency calibration. The idler (3.2–3.9 μm) is locked with the Pound-Drever-Hall (PDH) technique to a 1.9-m-long optical cavity consisting of two 1 m radius of curvature concave Si mirrors dielectric coated for 99.7% reflectivity over 3.1–3.4 μm surrounding a plasma cell. Cavity reflection and transmission are monitored by photodiodes (Boston Electronics Vigo PVM-10.6-1x1) with an effective bandwidth of ~125 MHz.

Heterodyne and PDH sidebands are generated by applying voltages at their respective frequencies to the fiber EOM on the seed laser simultaneously. The resultant frequency spectrum of the pump laser is imprinted on the idler beam. A PDH error signal used for cavity locking is generated by demodulating the cavity reflection signal at the frequency RF1 (typically 2–20 MHz). The error signal is sent to feedback electronics which stabilize the length of the cavity on slow timescales via a piezoelectric transducer (PZT) attached to one of the cavity mirrors, and apply fast corrections to the idler frequency by a PZT mounted to one of the signal cavity mirrors inside the OPO head. The cavity transmission detector signal is sent to a pair of mixers ~90° out of phase with one another, and each is demodulated at frequency RF2 (equal to the cavity FSR of 79.12 MHz). The overall phase of the heterodyne detection is adjusted by phase shifting the RF signal driving the EOM using cables of appropriate lengths. The demodulated signal from each mixer is then sent to a lock-in amplifier referenced to twice the frequency used to drive the plasma, and the in-phase and quadrature outputs of each amplifier are digitized and stored on a computer.

Ions are produced in a liquid-nitrogen-cooled multi-inlet multi-outlet positive column discharge cell, which is placed between the two free-standing mirrors of the optical cavity [18]. Intracavity radiation is admitted into the cell by means of CaF_2 windows aligned at Brewster's angle. The plasma is driven by a 40 kHz sine wave voltage produced by amplifying the output of an arbitrary waveform generator with an audio amplifier (Techron 7780) and a step-up transformer. H_3^+ was produced at a pressure of 200 mTorr and a discharge current of 170 mA. The outputs of the two mixers were each demodulated at 80 kHz with a lock-in amplifier set to a 10 ms time constant (16 Hz detection bandwidth).

Typical operation begins by filling the cooling jacket of the cell with liquid nitrogen and igniting the plasma. The cavity length is adjusted to bring it into resonance with the laser, and the laser-cavity lock is established. The idler frequency is tuned by applying a voltage to an internal PZT on the YDFL, and the cavity length is
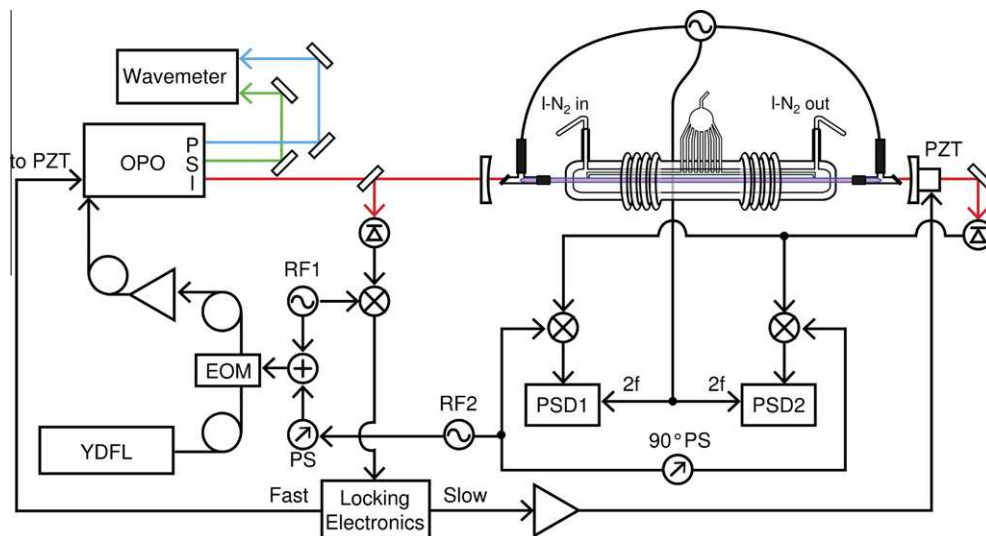
Figure 1. Block diagram of NICE-OHVMS instrument. Details of its operation are given in the main text. YDFL: Ytterbium-doped fiber laser; EOM: electro-optic modulator; OPO: optical parametric oscillator with pump (P, blue), signal (S, green) and idler (I, red) beams; PZT: piezoelectric transducer, PS: phase shifter; PSD: phase sensitive detector; •: signal splitter.

controlled with the locking electronics to maintain the resonance condition. When the cavity PZT reaches the end of its travel, the laser-cavity lock is electronically interrupted, the cavity length is reset to the other end of its travel, a new resonance is found, and the lock is reestablished. In this manner, the spectrometer can scan without manual intervention over the entire range of the YDFL PZT (around 100 GHz), although in practice a scan is generally much shorter. It is in principle possible to extend the automated tuning range further by electronic control of the intracavity etalon of the OPO and the nonlinear crystal position/temperature, but the practical utility of such efforts would likely be minimal.

3. Results and analysis

3.1. Lineshapes

The overall Doppler lineshape for NICE-OHVMS in both absorption and dispersion has odd symmetry, and qualitatively appears similar to the third derivative of a Gaussian absorption profile. A detailed analysis of the lineshape is beyond the scope of this Letter and will be the subject of a future work, but a qualitative description follows. Consider a general NICE-OHMS lineshape such as that shown in panels a and b of Figure 2 in Ref. [8]. If the signal belongs to an ion, then the AC voltage of the plasma causes velocity modulation (VM), Doppler shifting the lineshape at the plasma frequency. As a result of the bidirectional nature of light in our optical cavity, the lineshape is simultaneously Doppler shifted to the red and to the blue by the same amount at each point in time along the plasma voltage cycle. Consequently, the time-dependent signal repeats itself every plasma half-cycle, or at twice the AC plasma frequency ($2f_{vm}$). In addition to VM, an ion also experiences concentration modulation (CM) at $2f_{vm}$, and CM may be phase shifted with respect to VM. Thus, in addition to a periodic Doppler shift at $2f_{vm}$ from VM, the lineshape amplitude varies at $2f_{vm}$ from CM. The net signal observed comes in 4 channels corresponding to the even and odd second order Fourier coefficients of the absorption and dispersion profiles affected by VM and CM.

The sub-Doppler lineshape is more straightforward. As has been discussed in regard to previous NICE-OHMS setups [19,20,9], the carrier and sidebands can each act as pumps and probes for saturation spectroscopy. The Lamb dips arising from the Bennet holes burned in the population appear at half-integer multiples of the
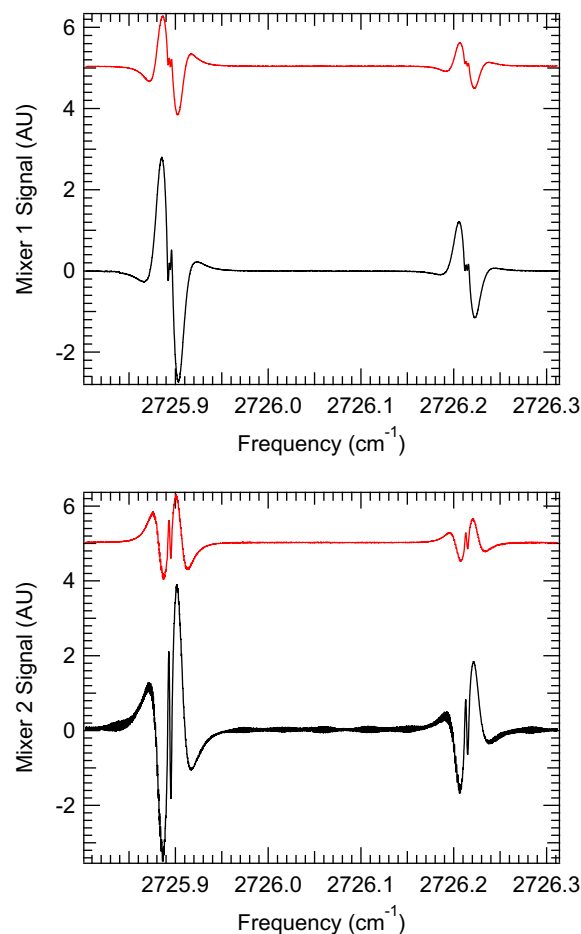

Figure 2. NICE-OHVMS spectrum of the $R(1,0)$ and $R(1,1)^u$ transitions of the v_2 fundamental band of H_3^+. Each panel shows the in-phase (black, bottom) and quadrature (red, top) outputs of a lock-in amplifier demodulating the indicated mixer's signal.

carrier-sideband spacing f_h, i.e., at all frequencies at which forward- and reverse-propagating beams sample the same velocity component of the Doppler distribution. At the line center v_0, when the

zero-velocity distribution is both pumped and probed by the carrier, a signal only appears in dispersion as the heterodyne detection scheme employed by NICE-OHMS is insensitive to absorption of the carrier. In the current work, the heterodyne modulation index (β) is small enough (~ 0.63) that only the carrier has sufficient power to saturate transitions, while the sidebands can only act as probes. The dispersion signal therefore contains Lamb dips at v_0 and $v_0 \pm f_h/2$, while the absorption signal contains them at $v_0 \pm f_h/2$.

While VM and CM have a strong influence on the lineshape of the Doppler profile, they do not affect the sub-Doppler features in the same way. Because Bennet holes are only burned in the population at or spaced evenly around the zero-velocity component of the ion distribution, VM effectively changes the abundance of ions with the appropriate velocity. In that way, VM effectively behaves like CM, and the net effect is to influence the amplitude of the Lamb dip lineshape and the relationship between the amplitudes of the even and odd Fourier coefficients within absorption or dispersion. Neglecting any change of the ions' collision rate with changing velocity, VM and CM do not affect the sub-Doppler profile beyond its amplitude. The sub-Doppler lineshape function [9] is

$$\chi(v_d) = \left(A_1 \left[\chi_a \left(v_d - \frac{f_h}{2} \right) - \chi_a \left(v_d + \frac{f_h}{2} \right) \right] \right) \sin \theta_h$$
$$+ \left(-2A_0 \chi_d(v_d) + A_1 \left[\chi_d \left(v_d - \frac{f_h}{2} \right) + \chi_d \left(v_d + \frac{f_h}{2} \right) \right] \right) \cos \theta_h, \quad (1)$$

where v_d is the frequency detuning from the transition center frequency, θ_h is the heterodyne detection phase, A_0 is the effective amplitude of the central (carrier-carrier) dispersion Lamb dip, and A_1 is the effective amplitude of the carrier-sideband Lamb dips for absorption and dispersion. $\chi_a(\omega)$ is a Lorentzian lineshape function for absorption, and $\chi_d(\omega)$ is a lineshape function for dispersion related to $\chi_a(\omega)$ by the Kramers–Kronig relations. These are defined as

$$\chi_a(\omega) = \frac{1}{1 + \gamma^2(\omega - \omega_0)^2} \quad \text{and} \quad \chi_d(\omega) = \frac{-(\omega - \omega_0)\gamma}{1 + \gamma^2(\omega - \omega_0)^2},$$

where ω_0 is the center and γ is the inverse of the half-width at half-maximum. When using this fit function, f_h is held at the cavity FSR (79.12 MHz), the amplitudes are constrained such that $A_0 > A_1$, and the Doppler profile near the line center is approximated by a third-order polynomial with the quadratic term set to 0.

3.2. H_3^+ Spectra

A sample spectrum of the $R(1,0)$ and $R(1,1)^u$ transitions of the v_2 fundamental band of H_3^+ is shown in Figure 2. The signals in the top and bottom panels are the demodulated in-phase (black) and quadrature (red, offset) components of the two mixers, which in our setup we measure to be 96° out of phase with one another. The in-phase components of the $R(1,0)$ transition are shown in greater detail in Figure 3. The overall lineshape is slightly asymmetric; the blue side of the transition is stronger than the red side, particularly in mixer 2. The origin of this asymmetry is unknown, and its impact on the spectroscopic accuracy will be discussed below.

A simultaneous fit of the $R(1,0)$ sub-Doppler features in all four detection channels to Eq. (1) is shown in Figure 4. A number of constraints were employed to ensure that the fit parameters were all internally consistent. The line center frequency and Lamb dip width were forced to be equal for all four data channels. Mixers 1 and 2 were held at 96° apart, and the sideband spacing was held equal to the cavity FSR of 79.12 MHz. Because the in-phase and quadrature components of each mixer sample different blends of CM and VM, the Lamb dip amplitudes were allowed to be different for the in-phase channels and the quadrature channels. However, the two in-phase channels were forced to have equal Lamb-dip amplitudes, and likewise for the two quadrature channels. After all of these
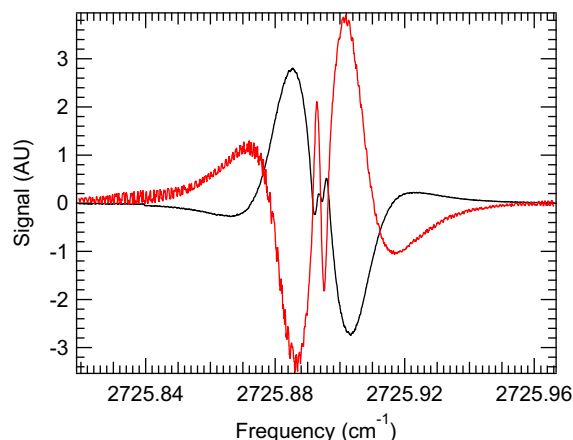

Figure 3. NICE-OHVMS spectrum of the $R(1,0)$ transition of the v_2 fundamental band of H_3^+. The black trace is the in-phase output of mixer 1, and the red is the in-phase output of mixer 2.
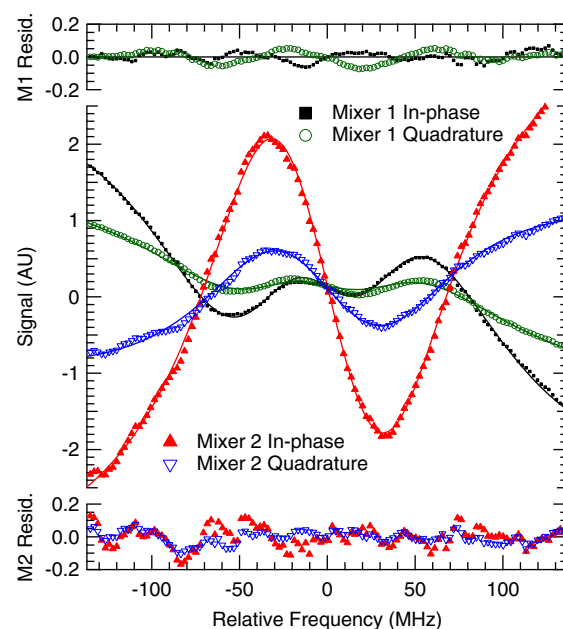

Figure 4. A simultaneous fit of the central sub-Doppler region of the H_3^+ $R(1,0)$ transition from all four data channels to Eq. (1). The symbols in the central portion of the graph are the data, and the solid lines are the fit results. The residuals of the fits are shown in the upper panel for mixer 1 and in the lower panel for mixer 2; in each case the symbols correspond to those in the central panel.

constraints, there are a total of 19 fit parameters for the entire data set: the line center frequency v_0, the Lamb dip full width at half maximum ($2/\gamma$), the overall detection phase θ_h, Lamb dip amplitudes A_0 and A_1 for the in-phase channels and the quadrature channels, and baseline terms of the form $c_0 + c_1 x + c_3 x^3$ to approximate the central portion of the Doppler profile in each channel.

The overall quality of the fit is quite good; the residuals are composed primarily of fringing evident on top of the spectrum (especially mixer 2) with the notable exception of the quadrature channel of mixer 1, which has some small systematic deviations on the Lamb dips. The line center v_0 derived from the fit is $2725.89401954 \pm 0.0000023$ cm^{-1}, but the absolute accuracy is limited by the $> 2 \times 10^{-3}$ cm^{-1} accuracy of the wavemeter, so the exact frequency should not be trusted. More important is the uncertainty of the line center determination, which is ~ 70 kHz; this represents the maximum potential accuracy of the technique provided suitable frequency calibration is made (but see the discussion

below about the effects of the asymmetry). The overall detection phase θ_h was found to be 132°, indicating a blend of absorption and dispersion in each mixer. Because the Lamb dip widths (full width at half maximum of ~110 MHz as indicated by our fit) are much broader than the Lamb dip spacing of 39.56 MHz ($f_h/2$), the individual Lamb dips for absorption and dispersion cannot be resolved at any RF detection phase. Rather than tuning the phase to separate absorption from dispersion in the two mixers, a phase of 132° was chosen because it was found to isolate the fringing as much as possible in a single detection channel (mixer 2 in-phase), thus minimizing the fringing in the other 3 channels.

4. Discussion

The most interesting aspect of the NICE-OHVMS technique is the presence of Lamb dips which enables high precision measurements of line center frequencies. Prior to the development of NICE-OHVMS, the only methods capable of routine sub-Doppler molecular ion spectroscopy utilized fast ion beams which, due to kinematic compression, give linewidths on the order of 10 to 120 MHz [21–23]. The linewidths from ion beams are comparable to the Lamb dips presented here, though the current work with a positive column has the advantage of much higher ion density than that within an ion beam.

With the H_3^+ Lamb dip linewidths of ~110 MHz demonstrated here, the precision of the line center determination is on the order of 70 kHz. In its present implementation, the technique's accuracy is limited by the wavemeter, and also by slow drifts in the frequency of the signal and idler beams caused by thermal fluctuations of the OPO cavity. Use of an optical frequency comb to stabilize and measure the frequencies of the pump and signal beams would reduce the accuracy uncertainty to < 100 kHz. Ultimately, the total uncertainty of the technique will be determined by the reproducibility of line center determinations once appropriately calibrated.

The asymmetry observed in the overall NICE-OHVMS lineshape can adversely affect the overall accuracy. As mentioned above, the origin of this asymmetry is unknown, although it varies with heterodyne detection phase; similar effects were not observed in the near-IR implementation of NICE-OHVMS [9]. Nevertheless, we have performed simulations of the effects of the asymmetry by synthesizing skewed profiles and comparing the results of our fit function to the actual location of the Lamb dips. Based on the fitting of our simulations, we estimate the magnitude of this line center shifting to be less than a few MHz, even for Doppler profiles that are much more asymmetric than those shown in this Letter. Further study of this phenomenon will be possible with an optical frequency comb, and such work is envisioned in the near future.

The width of the Lamb dips (~110 MHz FWHM from the fitting) is fairly broad. We have varied the intracavity laser power and the cell pressure, but any differences in the linewidth were not observable. However, the ranges of the power and pressure measurements were limited: the intracavity power could only be changed by a factor of 2 before the laser-cavity lock was adversely affected, and the plasma could only give stable operation over 200–600 mTorr. Such wide Lamb dips were also observed in the NICE-OHVMS experiment performed on N_2^+ in the near-IR [9]; in that study, the authors were able to observe a change in linewidth with pressure, but extrapolating to zero pressure still gave a linewidth of ~30 MHz. Assuming that the linewidth is related to the time an ion spends at zero velocity, it is perhaps unsurprising that a less massive ion like H_3^+ has a broader linewidth than N_2^+, as its velocity may be more easily altered by weak long-range interactions.

The fringing apparent in the figures above limits the sensitivity of the present measurements in 2 of the 4 detection channels. The origin of the fringing is not fully understood; however, it appears to have a definite phase with respect to both the heterodyne detection and the plasma modulation. When the plasma is turned off, the fringing does not appear in a scan, and if the cavity transmission detector is blocked while a signal originating from a single fringe is present on a lock-in channel, the signal vanishes. Thus, it appears that the fringing is the result of the plasma interacting with the laser light rather than a purely electronic effect. One possibility is that residual amplitude modulation (RAM) in the heterodyne sidebands is being modulated by the plasma. RAM is an imbalance in the amplitude and/or phase of the sidebands with respect to one another. When demodulated, RAM appears as a DC offset in the heterodyne signal; because of our detection scheme using velocity modulation and $2f$ detection, the NICE-OHVMS would ordinarily be insensitive to such an offset. However, if the refractive index of the plasma varies at $2f$, the DC signal from RAM will be modulated at $2f$ as well, resulting in a net NICE-OHVMS signal. Because RAM is also affected by the presence of etalons in the optical system and the optical frequency, a fringing pattern could possibly result as a function of laser frequency. Testing whether this is truly the origin of the fringing is difficult; however, it is probable that the fringing would be reduced by employing a RAM compensation scheme via temperature and voltage control of the fiber EOM [24].

The sensitivity of the technique at the experimental detection bandwidth of 16 Hz, as determined from the noise-equivalent absorption in the baseline of the in-phase component of mixer 1 (which has the least fringing of the four detection channels), is 3.4×10^{-9} cm^{-1}. which is about two orders of magnitude above the shot noise limit of 3.9×10^{-11} cm^{-1} calculated from

$$\alpha_{\min} = \frac{\pi}{2F} \sqrt{\frac{eB}{\eta P_0}} \frac{1}{J_0(\beta)J_1(\beta)L}, \tag{2}$$

where F is the cavity finesse (120), e the fundamental electric charge, B the detection bandwidth (16 Hz), η the detector responsivity, P_0 the power incident on the detector, $J_n(\beta)$ the nth order Bessel function for modulation index β (0.63), and L the cavity length (190 cm). While NICE-OHMS has been able to achieve a noise level within a factor of 2 of the shot noise limit in one implementation [7], the performance achieved by NICE-OHVMS relative to the shot noise limit is already comparable to a number of other NICE-OHMS setups (see the extensive discussion in Section 4 of [8]).

Ultimately, the absolute sensitivity can be improved by identifying and eliminating noise sources and by increasing the cavity finesse. An increase in cavity finesse leads to additional technical challenge in maintaining the laser-cavity lock, and may make the system even more susceptible to the fringing effects that have already been observed. Such challenges can likely be overcome by improving the bandwidth of the laser frequency corrections (currently limited to the 10 kHz bandwidth of the signal cavity PZT), and correcting for RAM as discussed above.

5. Conclusions

In this Letter, we have demonstrated sub-Doppler spectroscopy of molecular ions in the mid-infrared spectral region using the NICE-OHVMS technique with a cw-OPO. By phase modulating the seed laser with a fiber EOM prior to amplification and optical parametric oscillation, the mid-infrared idler is also phase modulated without requiring a mid-IR EOM. The high optical power of the idler beam allows use of high-bandwidth detectors, which in turn make ultra-sensitive spectroscopy via NICE-OHMS possible. Velocity modulation spectroscopy is then combined with NICE-OHMS to afford ion-neutral discrimination, and the intracavity laser power is sufficient for saturating fundamental rovibrational transitions as demonstrated by spectroscopy of H_3^+. By fitting the sub-Doppler spectral features, the center frequencies of individual rovibrational lines can be measured with a precision of 70 kHz, and the maximum

achieved sensitivity is within a factor of ∼90 of the shot noise limit. Improvements to the technique, such as addition of an optical frequency comb for accurate wavelength calibration, technical modifications to improve its sensitivity, and expanding the frequency coverage of the OPO from 3.2–3.9 μm to 2.8–4.8 μm, are envisioned.

References

[1] C.S. Gudeman, M.H. Begemann, J. Pfaff, R.J. Saykally, Phys. Rev. Lett. 50 (1983) 727.
[2] C.S. Gudeman, M.H. Begemann, J. Pfaff, R.J. Saykally, J. Chem. Phys. 78 (1983) 5837.
[3] S.K. Stephenson, R.J. Saykally, Chem. Rev. 105 (2005) 3220.
[4] B.M. Siller, A.A. Mills, B.J. McCall, Opt. Lett. 35 (2010) 1266.
[5] A.A. Mills, B.M. Siller, B.J. McCall, Chem. Phys. Lett. 501 (2010) 1.
[6] L.C. Sinclair, K.C. Cossel, T. Coffey, J. Ye, E.A. Cornell, Phys. Rev. Lett. 107 (2011) 093002.
[7] J. Ye, L.-S. Ma, J.L. Hall, J. Opt. Soc. Am. B 15 (1998) 6.
[8] A. Foltynowicz, F. Schmidt, W. Ma, O. Axner, Appl. Phys. B 92 (2008) 313.
[9] B.M. Siller, M.W. Porambo, A.A. Mills, B.J. McCall, Opt. Exp. 19 (2011) 24822.
[10] M.S. Taubman, T.L. Myers, B.D. Cannon, R.M. Williams, Spectrochim. Acta 60 (2004) 3457.
[11] M.W. Porambo, B.M. Siller, J.M. Pearson, B.J. McCall, Opt. Lett., in press.
[12] W.D. Watson, Astrophys. J. 183 (1973) L17.
[13] E. Herbst, W. Klemperer, Astrophys. J. 185 (1973) 505.
[14] T. Oka, Phys. Rev. Lett. 45 (1980) 531.
[15] C.M. Lindsay, B.J. McCall, J. Mol. Spectrosc. 210 (2001) 60.
[16] C.P. Morong, J.L. Gottfried, T. Oka, J. Mol. Spectrosc. 255 (2009) 13.
[17] L. Velilla, B. Lepetit, A. Aguado, J.A. Beswick, M. Paniagua, J. Chem. Phys. 129 (2008) 084307.
[18] C. Lindsay, E.T. White, T. Oka, Chem. Phys. Lett. 328 (2000) 129.
[19] A. Foltynowicz, W. Ma, O. Axner, Opt. Exp. 16 (2008) 14689.
[20] O. Axner, W. Ma, A. Foltynowicz, J. Opt. Soc. Am. B 25 (2008) 1166.
[21] C.S. Gudeman, R.J. Saykally, Ann. Rev. Phys. Chem. 35 (1984) 387.
[22] J.V. Coe, J.C. Owrutsky, E.R. Keim, N.V. Agman, D.C. Hovde, R.J. Saykally, J. Chem. Phys. 90 (1989) 3893.
[23] A.A. Mills, B.M. Siller, M.W. Porambo, M. Perera, H. Kreckel, B.J. McCall, J. Chem. Phys. 135 (2011) 224201.
[24] I. Silander, P. Ehlers, J. Wang, O. Axner, J. Opt. Soc. Am. B 29 (2012) 916

Brian Siller graduated with a B.A. in Chemistry, Computer Science, and Mathematics from Ohio Wesleyan University in 2007, and is currently pursuing a Ph.D. in Physical Chemistry at the University of Illinois.

Adam Perry graduated with a B.S. in Chemistry from Oregon State University in 2011, and is currently a graduate student in Physical Chemistry at the University of Illinois.

Joe Kelly graduated with a B.S. in Chemistry from the University of Illinois in 2012.

Paul Jenkins II is currently pursuing his B.S. in Chemical Engineering at the University of Illinois, and plans to graduate in 2015.

Ben McCall received his Ph.D. from the University of Chicago in Chemistry and Astronomy & Astrophysics. Following a Miller Research Fellowship at the University of California at Berkeley, he joined the faculty of the University of Illinois, where he is currently an Associate Professor of Chemistry and Astronomy.

Kyle Crabtree graduated with a B.S. in Chemistry from Ball State University in 2006, and received his Ph.D. in Chemistry from the University of Illinois in 2012. He is currently a CfA Postdoctoral Fellow at the Harvard-Smithsonian Center for Astrophysics.

James Hodges received a B.S. in Chemistry and a B.S. in Polymer & Fiber Chemistry in 2010 from Clemson University. He currently attends the University of Illinois pursuing a PhD in Chemistry as a Springborn Fellow and an NSF Graduate Research Fellow.

Indirect Rotational Spectroscopy of HCO+

Brian M. Siller,[†] James N. Hodges,[†] Adam J. Perry,[†] and Benjamin J. McCall*,[†,‡]

[†]Department of Chemistry and [‡]Departments of Physics and Astronomy, University of Illinois at Urbana−Champaign, Urbana, Illinois 61801, United States

ABSTRACT: Spectroscopy of the ν_1 band of the astrophysically relevant ion HCO+ is performed with an optical parametric oscillator calibrated with an optical frequency comb. The sub-MHz accuracy of this technique was confirmed by performing a combination differences analysis with the acquired rovibrational data and comparing the results to known ground-state rotational transitions. A similar combination differences analysis was performed from the same data set to calculate the previously unobserved rotational spectrum of the ν_1 vibrationally excited state with precision sufficient for astronomical detection. Initial results of cavity-enhanced sub-Doppler spectroscopy are also presented and hold promise for further improving the accuracy and precision in the near future.
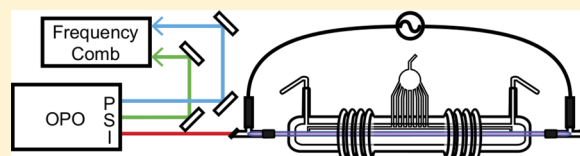
INTRODUCTION

Molecular ions are a particularly challenging group of species to study with optical spectroscopy. Even in laboratory plasmas that are designed to observe only a specific ion, neutral molecules are still orders of magnitude more abundant than their charged counterparts. This is why the most productive techniques for ion spectroscopy tend to have some method for discriminating ionic absorption signals from neutral ones. Since the late 1980s, the predominant tool for this has been velocity modulation spectroscopy (VMS). The groundwork of VMS was laid by Wing et al. in a velocity modulated ion beam,[1] and the first application of VMS as it is known today was by Gudeman et al. in a velocity modulated positive column discharge cell.[2] Since the initial work, the technique has become a mainstay in ion spectroscopy and has been extensively reviewed.[3,4]

Protonated carbon monoxide, HCO+, was the first ion whose spectrum was acquired using VMS. The R-branch of the ν_1 C−H stretch band was first measured by Gudeman et al. in a positive column discharge cell out to R(18).[2] Shortly after, the P-branch was also observed out to P(10) in a modulated DC glow.[6] After these lines were published, it was another 24 years before any work revisited the ν_1 band, when Verbraak et al. used a continuous wave optical parametric oscillator (cw-OPO) operating in the mid-infrared and a supersonic expansion discharge source to rotationally cool the ions.[7]

The first observation of an HCO+ rotational transition was via telescope rather than in a laboratory in 1970 by Buhl and Snyder.[8] Because the line that they observed was unidentified at the time, it was referred to as "X-ogen". Later that year, Klemperer suggested that the X-ogen line was due to the $J = 1 \leftarrow 0$ transition of HCO+.[9] Five years later, Woods et al. confirmed its identity by microwave spectroscopy.[10] Since that time, HCO+ has been found in a variety of astronomical environments including protoplanetary nebulae,[11] star forming regions,[12] the interstellar medium,[13] and even the comet Hale−Bopp.[14] The abundance of HCO+ makes it an important

participant in the rich chemistry that exists in the interstellar medium. Because of the large rotational constant of HCO+, its higher rotational transitions exist in the submillimeter/terahertz region. Newer telescopes such as the Atacama Large Millimeter and submillimeter Array (ALMA) and the Stratospheric Observatory For Infrared Astronomy (SOFIA) have submillimeter/terahertz capability. These new astronomical capabilities lend necessity to a relatively simple way to gain laboratory information in that spectral region, a challenging region for laboratory spectroscopy, due in part to the relative scarcity of quality sources and detectors compared to the microwave and infrared spectral regions. In this work, we present a demonstration of how precision rovibrational spectroscopy can be used to infer rotational transitions to precision sufficient to facilitate astronomical searches.

In the case of HCO+, most of the ground state transitions have been observed up to $J = 17 \leftarrow 16$, with the exception of a few gaps in coverage.[15] Additionally, only a few pure rotational lines have been observed in vibrationally excited states. One such transition is the $J = 3 \leftarrow 2$ rotational transition in the ν_1 first vibrationally excited state.[16] With this single transition combined with our high-precision IR spectrum, the entire rotational spectrum of the ν_1 state can be calculated, limited only by the number of rovibrational lines that have been observed. The technique demonstrated here is also useful for determining high precision rotational constants in excited states.

In this work, we present spectra of the ν_1 fundamental band of HCO+ acquired using optical heterodyne spectroscopy coupled with VMS (OH-VMS). This technique combines the advantages of the low noise of heterodyne spectroscopy with
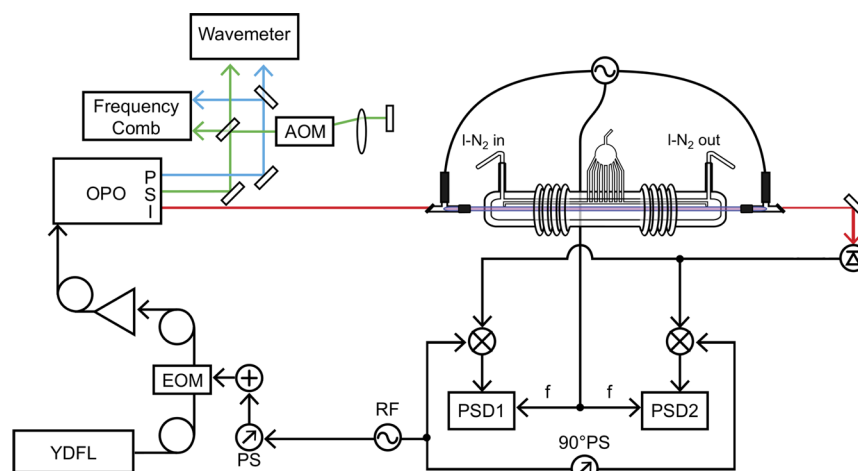
Figure 1. Experimental layout. YDFL, ytterbium-doped fiber laser; EOM, electro-optic modulator; PS, phase shifter; RF, radio frequency generator; OPO, optical parametric oscillator; P,S,I, pump, signal, idler; AOM, acousto-optic modulator; PSD, phase-sensitive detector.

the ion-neutral discrimination of VMS. Our instrument utilizes a cw-OPO tunable from 3.2 to 3.9 μm, and produces ions within a liquid nitrogen cooled positive column discharge cell. Optical frequency comb calibrated scans were acquired and fit with sub-MHz precision, and the resulting fits were used to calculate rotational transitions for the ground state and the first vibrationally excited C−H stretch state. These calculations result in the first experimental observation, albeit indirectly, of the $J = 3 \leftarrow 2$ transition in the ground state and the complete determination of the rotational spectrum up to $J = 10 \leftarrow 9$ in the ν_1 first excited state.

■ EXPERIMENTAL SECTION

The experimental setup, shown in Figure 1, has been described previously[17] with the exception of the frequency comb integration, so it will be discussed only briefly here. A Ytterbium-doped fiber laser is frequency modulated with a fiber-coupled electro optic modulator (EOM) using two RF generators: one at ∼80 MHz for heterodyne detection, and the other at ∼2 MHz for locking to the optical cavity around the discharge cell. After the modulation is applied, this seed laser is amplified to 10 W total power using a fiber amplifier, and this amplified beam acts as the pump for the optical parametric oscillator (OPO).

Three beams exit the OPO head: the pump (∼1064 nm), the signal (tunable from 1.5 to 1.6 μm), and the idler (tunable from 3.2 to 3.9 μm). The idler is used for spectroscopy of HCO^+, while the other beams are used for frequency measurements using a near-infrared wavemeter and frequency comb. For the comb-calibrated scans, the wavemeter is only used prior to a scan to determine which comb modes the pump and signal are each closest to, while the comb is used throughout the scan to take frequency readings at each acquired data point.

Comb Integration. The optical frequency comb used in this work (Menlo FC1500) has been described previously in operation with a different laser system.[18] In this work, the comb is used for both stabilizing and measuring the pump frequency. It is also used for measuring the frequency of the signal after it is shifted by a double-pass AOM. The shifted-signal frequency and the AOM frequency are then used to calculate the unshifted signal frequency, which when combined with the pump frequency measurement, are used to determine the

frequency of the idler. A detailed explanation of the comb operation follows.

Scanning the OPO with the comb is accomplished by first tuning the carrier-envelope offset of the comb to approximately 20 MHz and determining its sign. Then the comb repetition rate is tuned to make the signal offset beat lie within the range of 25−35 MHz from the nearest comb mode, limited by the RF bandpass filter built into the frequency counter used to record that beat. Then the frequency of the pump is tuned to approximately 20 MHz from its nearest comb mode, and the signs of the offset beats for both the pump and the signal are determined and recorded. Finally, the pump is offset-locked to the comb using a frequency-to-voltage converter circuit that generates an appropriate error signal for offset locking.

The nearest comb mode numbers are determined for the pump and the signal before each scan using the wavemeter, then are recorded (and incremented/decremented for the signal when necessary) as the scan progresses. At each frequency step, the data acquisition program pauses for 1.5 s, then the comb repetition rate and offset beats are recorded by frequency counters with 1 Hz refresh rates, and the lock-in amplifier outputs are recorded. With the lock-in amplifier time constant set to 300 ms, the lock-in amplifiers have 5 time constants to respond before the reading is polled for each point, so any scanning direction dependent line center pulling is smaller than the random scan-to-scan variability in line center determination.

After each point, the repetition rate is tuned by an amount sufficient to slew the pump frequency by ∼5 MHz (∼1.8 Hz change in repetition rate). The pump remains offset locked to the same comb mode throughout the course of each scan. The total continuous scanning range of the pump (and therefore for the idler) for comb-calibrated scans is limited to ∼800 MHz by the comb scanning electronics; the comb repetition rate can only be changed by a relatively small amount while still retaining its lock onto the direct digital synthesizer (DDS) that stabilizes the repetition rate.

To keep the signal offset within the frequency counter bandpass filter at each point, a feed-forward system is used to tune the signal frequency using a double-pass acousto-optic modulator (AOM) setup. In a double-pass configuration, the frequency shift induced by the AOM is doubled, while making the pointing of the beam independent of the frequency applied

to the AOM.[19] Stable pointing is crucial to the operation of the system, as good spatial overlap between the comb light and each of the cw beams is important for generating offset beat signals on the high speed detectors.

After the counters are read for a data point and the repetition rate is slewed to the next point, the amount the signal frequency needs to be shifted by is calculated using the change in the repetition rate, the signal comb mode number, and the amount the signal was away from the 30 MHz target offset frequency for the previous point; this frequency shift is then applied to the frequency of the RF generator that drives the AOM. The AOM diffraction efficiency is high enough to provide reliable signal/comb offset beat measurements in the driving frequency range of 150−210 MHz, which corresponds to a frequency shift of 300−420 MHz when taking into account the double-pass configuration. When the calculated desired AOM frequency lies outside this range, the drive frequency is shifted by 50 MHz (corresponding to a 100 MHz change in the shifted signal frequency, matching the comb repetition rate), and the signal mode number is incremented or decremented by one, depending on whether the 100 MHz shift was positive or negative.

This signal-shifting scheme allows the shifted signal frequency to be determined using the frequency comb at each point, despite the fact that the signal frequency is fixed (with the exception of some slow drift) while the comb repetition rate is slewing. The unshifted signal frequency can then be determined simply by subtracting the AOM frequency shift, which is precisely known from the digital setting of the RF generator at each point, and this unshifted signal frequency is subtracted from the directly measured pump frequency to determine the idler frequency.

Spectroscopic Configuration. The plasma cell used in this work, Black Widow, shown in Figure 2, was the same cell
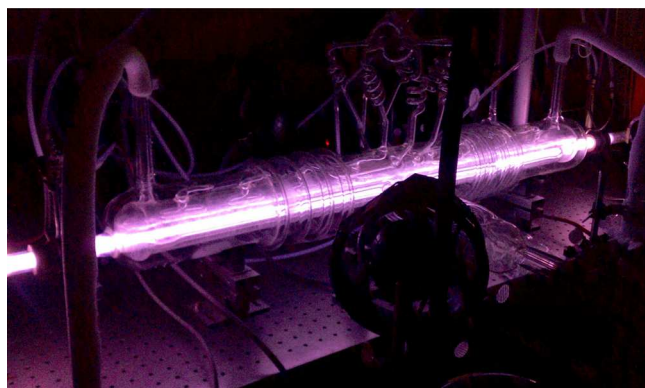

Figure 2. Black Widow, the liquid nitrogen cooled positive column discharge cell acquired from Takeshi Oka and used for the work in this article. The central bore, where the plasma discharge occurs, is surrounded by a sheath of flowing liquid nitrogen, which is in turn surrounded by a vacuum jacket to prevent ice from forming on the cell.

used by Takeshi Oka in many of his velocity modulation experiments. It allows for liquid nitrogen cooling of the plasma to reach an estimated rotational temperature of ~166 K for HCO$^+$, as shown in the Boltzmann plot in Figure 3, using plasma conditions of 30 mTorr CO in 500 mTorr H$_2$ with a 35 kHz, 140 mA discharge. The idler beam is coupled through Brewster windows on either end of the cell into the central bore
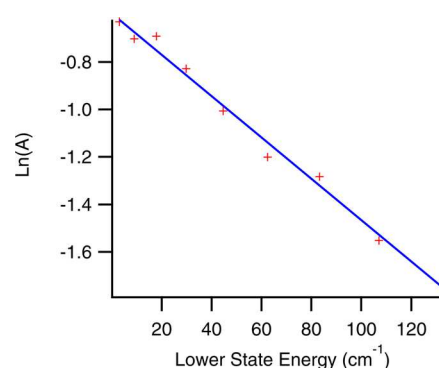

Figure 3. Boltzmann plot for R(1) through R(9), with the slope indicating a rotational temperature of ~166 K. The vertical axis is the natural log of the line strength normalized peak-to-peak amplitude of a double-pass scan for each transition.

of the discharge cell. For this work, three different optical configurations were used: single-pass, double-pass, and cavity-enhanced, all of which relied on heterodyne modulation and detection at ~80 MHz.

The comb calibrated scans presented in this article used a simple single-pass configuration, as shown in Figure 1. This allowed for the acquisition of Doppler-broadened scans with signal-to-noise ratios of ~300 for the strongest lines and ~100 for the weakest ones but, because of the lack of a bidirectional beam and sufficient laser power, did not allow for the observation of Lamb dips. A typical comb-calibrated scan is shown in Figure 4.
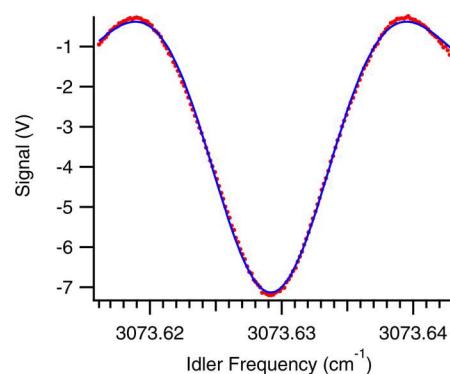

Figure 4. Typical comb-calibrated scan (red dots) of the P(5) transition of HCO$^+$, along with a fit to the data (blue line). Error bars for the points are not shown, as they would be smaller than the point size for both intensity and frequency.

A series of double-pass wavemeter-calibrated scans were collected for the previously unobserved P(11) through P(17) transitions. In the double-pass configuration, a single mirror was placed on the far side of the cell to back-reflect the idler for a second pass through the cell. Approximately 30% of the reflected beam was then picked off with a silicon window and directed to a high-speed detector, the signal from which was demodulated first at the heterodyne frequency, then at twice the plasma frequency (2f), as opposed to the 1f demodulation that was used for the single-pass work.

A few uncalibrated scans were collected with the laser frequency locked to an optical cavity positioned around the discharge cell, in a noise immune cavity enhanced optical heterodyne velocity modulation spectroscopy (NICE−

OHVMS)[20] configuration, as was done by Crabtree et al.[17] One such scan, showing strong central Lamb dip features on top of the Doppler profile, is shown in Figure 5. In this experiment,
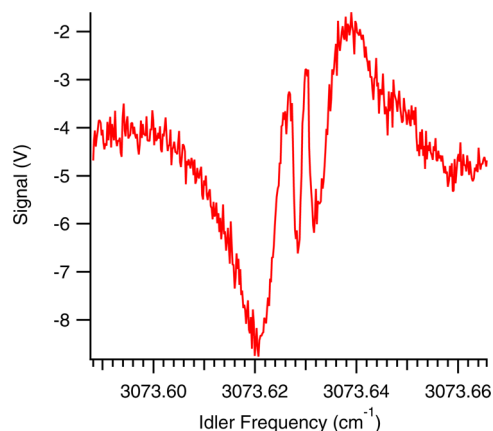

Figure 5. Roughly calibrated scan of the P(5) transition of HCO+, showing the Lamb dips that are obtainable with cavity enhancement combined with lower cell pressure. The frequency calibration of this scan was based on the line center determined from the comb calibrated scans combined with the approximate scan voltage to frequency transfer function of the seed laser.

cavity enhancement is combined with 2f demodulation, making detection sensitive to not only velocity modulation but also concentration modulation of the ions of interest. This detection scheme allows for the observation of Lamb dips as the zero-velocity population of ions is modulated throughout the course of a discharge cycle.

Unfortunately, the dielectric coatings on the mirrors were found to be hygroscopic, which led to poor laser coupling efficiency through the cavity in this wavelength range and degraded performance over time. To obtain optimal Lamb dip depth, the total cell pressure had to be decreased to ~200 mTorr, and the discharge current had to be turned down as low as possible while still maintaining a stable plasma, to ~100 mA. Both the lower pressure and the lower discharge current produce lower overall density of HCO+ within the cell. This decreased density combined with the poor laser transmission through the cavity cause the signal-to-noise in the NICE–OHVMS scans to be significantly compromised compared to the single- and double-pass scans, despite the factor of ~400 greater path length that NICE–OHVMS provides through the plasma.

■ RESULTS AND DISCUSSION

Each comb calibrated scan was fit to a second derivative of a Gaussian function, which approximates the convolution of heterodyne modulation with velocity modulation observed in the experiment. As can be seen in Figure 4, the fit is not perfect, especially near the outer lobes of the line shape. Lineshapes in velocity modulation experiments are often significantly more complex than simple derivatives of ordinary unmodulated lineshapes,[5] but for the purposes of determining line centers, the chosen function is sufficient. Between 4 and 7 scans were acquired of each transition, and the data acquired from those fits were used to compute the average line centers and standard errors shown in Table 1. The errors varied somewhat from one transition to the next, but the average uncertainty was found to be ~600 kHz.

Table 1. List of the Comb-Calibrated HCO+ Transition Center Frequencies (With Associated Uncertainties) Observed in the Current Work, Compared with Previous Measurements

transition	line center (cm⁻¹)	previous work[6] (cm⁻¹)	previous − current (MHz)
R(0)	3091.690432(16)	3091.6919(10)	44
R(1)	3094.618099(27)	3094.6181(10)	0
R(2)	3097.522054(07)	3097.5223(10)	7
R(3)	3100.402249(25)	3100.4034(10)	35
R(4)	3103.258604(21)	3103.2586(10)	0
R(5)	3106.090956(19)	3106.0909(10)	−2
R(6)	3108.899376(20)	3108.9002(10)	25
R(7)	3111.683680(04)	3111.6841(10)	13
R(8)	3114.443835(05)	3114.4445(10)	20
R(9)	3117.179881(41)	3117.1800(10)	4
P(1)	3085.763903(23)	3085.7646(10)	21
P(2)	3082.765487(53)	3082.7662(10)	21
P(3)	3079.743422(15)	3079.7437(10)	8
P(4)	3076.698005(05)	3076.6977(10)	−9
P(5)	3073.629188(16)	3073.6291(10)	−3
P(6)	3070.537136(19)	3070.5377(10)	17
P(7)	3067.421924(37)	3067.4224(10)	14
P(8)	3064.283464(10)	3064.2834(10)	−2
P(9)	3061.122045(18)	3061.1226(10)	17
P(10)	3057.937606(08)	3057.9380(10)	12

As can be seen by the fit in Figure 4, this fit function is not perfect, likely due to imperfect setting of the detection phases. For this work, both the RF and plasma demodulation phases were set to maximize the signal-to-noise of a single detection channel out of the four channels that were acquired with each scan. It is likely that there is some dispersive component to the line shape function, rather than it being purely absorptive. It is also likely that the velocity modulation of the ions is not purely sinusoidal and that the lock-in demodulation is not exactly in phase with the velocity modulation, and both of these factors can also affect the overall line shape.

There is also a slight asymmetry in the observed line shapes for several of the scans that is not fully understood at this time. By adding a slightly sloped baseline to the data, we can make it significantly more symmetric and also make the fit slightly better. Symmetrizing the data in this way causes the determined line center to shift by less than 1 MHz for even the most asymmetric scans. Given that we do not know the physical cause of this phenomenon, we have taken the approach of manipulating the data as little as possible, so this symmetrizing was only done to estimate the potential error induced by the asymmetry.

When asymmetry is present, it tends to manifest with the low-frequency lobe of the line shape having a greater maximum than the high-frequency one, although by tuning detection phases and plasma conditions, we are able to reverse the asymmetry, making the high-frequency lobe larger. Fitting the same line with opposite asymmetry slopes provides line centers that are shifted by less than 1 MHz relative to one another, providing further evidence that any asymmetry-induced errors in line center determination must be fairly small, on the order of 1 MHz or smaller.

All of the comb-calibrated data presented in this work was performed with the identical phase settings and plasma conditions, leading to line shapes that were similarly

asymmetric. Such a systematic error would be mitigated by subtraction of observed line centers, as is done in the combination differences analysis described in the following several paragraphs. On the basis of the errors in the calculation of rotational transitions, it appears that random scan-to-scan variability is the limiting factor in line center determination and not the effects of this asymmetry.

For approximately half of the comb-calibrated scans, the determined line centers disagreed with the previously measured HCO^+ transition frequencies[6] by greater than the specified accuracy of 30 MHz. It was found that the source of the errors was incorrect comb mode number determination for either the signal or the pump beams due to inaccuracy of the wavemeter. These incorrectly calibrated scans were easily corrected by adding or subtracting a multiple of the comb repetition rate to or from the calculated idler frequency. After correcting the idler frequency calibration, it was found that all but two of the observed transitions agreed with Amano's previous work to within 30 MHz. The two exceptions to the 30 MHz agreement were the R(0) and R(3) transitions, but those were both further verified by comparing the combination difference analysis with directly measured rotation transitions, as shown in Table 2. Any remaining error in the determination of comb mode numbers would appear as an error of ~100 MHz, which is not observed.

Table 2. Indirectly Calculated Rotational Transition Frequencies Derived from the Data in Table 1 Compared to the Directly Measured Rotational Transitions Compiled by Cazzoli et al.[15]

J'	J''	calc freq (MHz)	obs freq[15] (MHz)	calc − obs (MHz)
0	1	n/a	89188.5247	n/a
1	2	178374.6(17)	178375.0563	−0.5
2	3	267557.0(19)	n/a	n/a
3	4	356732.3(19)	356734.2230	−2.0
4	5	445903.9(21)	445902.8721	1.0
5	6	535061.0(23)	535061.5810	−0.5
6	7	624207.4(26)	624208.3606	−1.0
7	8	713344.0(27)	713341.2278	2.8
8	9	802455.7(27)	802458.1995	−2.5
9	10	891558.4(27)	891557.2903	1.1

A combination differences analysis was performed to demonstrate the accuracy of our comb-calibrated rovibrational compared to known rotational transitions. First, frequencies of transitions sharing the same upper state energy level, e.g., R(0) and P(2), were subtracted from one another to generate ground state energy level spacings for pairs of energy levels separated by two rotational energy levels. For example, the $J = 2 \leftarrow 0$ spacing was calculated from $f_{R(0)} - f_{P(2)}$, the $J = 3 \leftarrow 1$ spacing was calculated from $f_{R(1)} - f_{P(3)}$, and so forth for all observed transitions up to the $J = 10 \leftarrow 8$ spacing.

Then the directly measured $J = 1 \leftarrow 0$ transition was subtracted from the $J = 2 \leftarrow 0$ energy level spacing to indirectly compute the $J = 2 \leftarrow 1$ rotational transition frequency. This computed frequency was then subtracted from the $J = 3 \leftarrow 1$ spacing to compute the $J = 3 \leftarrow 2$ transition frequency, and the process was repeated for higher rotational energy levels up to $J = 10 \leftarrow 9$. At each step, the calculated rotational transition from the previous step was used with a new energy level difference to compute a new rotational transition. The indirectly calculated rotational transitions in the current work are compared to the previously observed rotational transition frequencies in Table 2.

Such an analysis was also carried out for the ν_1 (C−H stretch mode) first vibrationally excited state. To our knowledge, the only directly observed rotational transition was $J = 3 \leftarrow 2$.[16] This single transition, combined with our rovibrational data, is sufficient to compute the expected rotational transitions from $J = 1 \leftarrow 0$ up to $J = 10 \leftarrow 9$, as shown in Table 5.

The rovibrational comb-calibrated data were also fit to a simple Hamiltonian to determine the constants shown in Table 3, where the quartic distortion terms for the lower and upper

Table 3. Molecular Constants (And Associated Uncertainties) Obtained from a Least Squares Fit of the Full Comb-Calibrated Rovibrational Data Set; Full Fit Results, Including the Associated Residuals, Are Given in Table 4

constant	value (MHz)
ν_0	92598065.20(19)
B''	44594.166(25)
B'	44240.297(27)
D''	−0.07784(49)
D'	−0.07760(49)
$H' = H''$	$-0.0269(28) \times 10^{-3}$

vibrational states were constrained to be equal to one another. The full results of the fit, showing the deviations of the data from the fit result, is shown in Table 4. The experimental data

Table 4. Full Results of the Least Squares Fit of the Full Comb-Calibrated Rovibrational Data Set

J'	J''	obs freq (cm^{-1})	calc freq (cm^{-1})	obs − calc (cm^{-1})
0	1	3091.690432(16)	3091.690368	0.000064
1	2	3094.618099(27)	3094.618083	0.000016
2	3	3097.522054(07)	3097.522065	−0.000011
3	4	3100.402249(25)	3100.402251	−0.000002
4	5	3103.258604(21)	3103.258575	0.000030
5	6	3106.090956(19)	3106.090968	−0.000012
6	7	3108.899376(20)	3108.899361	0.000015
7	8	3111.683680(04)	3111.683678	0.000002
8	9	3114.443835(05)	3114.443840	−0.000005
9	10	3117.179881(41)	3117.179764	0.000117
1	0	3085.763903(23)	3085.763992	−0.000089
2	1	3082.765487(53)	3082.765454	0.000033
3	2	3079.743422(15)	3079.743436	−0.000014
4	3	3076.698005(05)	3076.698000	0.000005
5	4	3073.629188(16)	3073.629214	−0.000026
6	5	3070.537136(19)	3070.537148	−0.000012
7	6	3067.421924(37)	3067.421874	0.000050
8	7	3064.283464(10)	3064.283471	−0.000007
9	8	3061.122045(18)	3061.122020	0.000025
10	9	3057.937606(08)	3057.937608	−0.000002

agree with the fit within 2σ for all but three of the observed transitions, and all of the data agree with the fit to within 4σ. This provides further evidence for the internal consistency of this rovibrational data set, and validation that the random errors that contribute to the statistical uncertainties are the limiting factor of the accuracy and precision (as oppposed to other effects that vary from one line to the next, such as the observed asymmetry in the lineshapes).

In addition to the comb-calibrated scans that were collected for the combination differences analysis, several previously unobserved P-branch transitions were recorded with only

wavemeter calibration. All but one of the linecenters determined from these scans fall within the expected 70 MHz uncertainty from the wavemeter calibration. The one exception, P(17), is thought to be off by more than the uncertainty due to an inaccurate signal wavelength reading caused by poor optical alignment of the wavemeter. These transitions, whose frequencies are given in Table 6, could not be used for

Table 5. Pure Rotational Transitions for the Vibrationally Excited ν_1 State of HCO$^+$, Calculated from the Rovibrational Data in Table 1 and the Directly Observed[21] $J = 3 \leftarrow 2$ Rotational Transition

J'	J''	calc freq (MHz)	uncertainty (MHz)
0	1	88486.7	1.9
1	2	176955.4	1.6
2	3	n/a	n/a
3	4	353900.7	0.9
4	5	442366.0	1.1
5	6	530813.3	1.3
6	7	619257.7	1.6
7	8	707676.3	1.9
8	9	796093.7	1.9
9	10	884477.9	2.4

Table 6. Previously Unobserved Wavemeter-Calibrated Scans of the P(11) through P(17) Transitions[a]

transition	obs (cm^{-1})	calc (cm^{-1})	obs − calc (MHz)
P(11)	3054.730	3054.73019(4)	−6
P(12)	3051.502	3051.49993(5)	62
P(13)	3048.245	3048.24688(6)	−57
P(14)	3044.969	3044.97111(7)	−63
P(15)	3041.672	3041.67269(8)	−21
P(16)	3038.354	3038.35169(9)	69
P(17)	3035.013	3035.00817(10)	145

[a]Uncertainties are ∼70 MHz, limited by the wavemeter uncertainties for the pump and signal frequencies added in quadrature. Calculations are based on ground state constants from Cazzoli et al.,[15] and excited state constants are determined from our comb-calibrated scans.

combination differences calculations because their corresponding R-branch transitions lie outside the tuning range of our current OPO module, though additional tuning could be obtained with other modules.

CONCLUSIONS

The current work demonstrates the ability of Doppler-broadened comb-calibrated velocity modulation spectroscopy to determine line centers with sub-MHz accuracy and precision. This accuracy has been verified by performing a combination differences analysis of the rovibrational data and comparing the results to the previously observed rotational spectrum of vibrational ground state HCO$^+$. The potential of extending the technique to sub-Doppler work has also been demonstrated. With a proper set of cavity mirrors, it should be possible to further improve the precision of this technique. From the current series of fits, the Doppler-limited line width is ∼450 MHz, and the uncertainty of a single fit is ∼350 kHz. From the Lamb dip scan of HCO$^+$ shown in Figure 5, the peak-to-peak line width of the central sub-Doppler feature is only ∼50 MHz, so it is reasonable to assume that the precision of a fit to sub-Doppler features would be approximately an order of

magnitude more precise than one to a Doppler-broadened scan, assuming the S/N problem can be solved by a non-hygroscopic set of cavity mirrors. The investigation into whether the accuracy is also improved by the same factor will be the subject of future work.

One of the greatest advantages of this indirect approach over direct rotational spectroscopy is the generality of it. The chemistry within positive column discharge cells tends to be very rich, so it is possible to make a wide variety of molecular ions. The cell used in the current work was cooled with liquid nitrogen, but it could easily be cooled by water or air, or even heated to attain greater population in higher rotational levels and compute the rotational spectrum up to very high J values. The infrared source and detectors are also very versatile in terms of spectral coverage; entire rovibrational bands for a wide variety of ions lie within its tuning range and can be observed without any changes to the optoelectronic system.

This work also has implications for astronomical searches for the astrophysically relevant ion HCO$^+$. While the ground vibrational state has been thoroughly studied, little work has previously been done in this vibrationally excited state. Rotational transitions in the vibrationally excited state could be of astrophysical interest, particularly in hot, dense environments such as hot cores and circumstellar envelopes.[22]

AUTHOR INFORMATION

Corresponding Author

*(B.J.M.) E-mail: bjmccall@illinois.edu.

Notes

The authors declare no competing financial interest.

REFERENCES

(1) Wing, W.; Ruff, G.; Lamb, W.; Spezeski, J. Observation of the Infrared Spectrum of the Hydrogen Molecular Ion HD$^+$. *Phys. Rev. Lett.* **1976**, 36, 1488−1491.

(2) Gudeman, C. S.; Begemann, M. H.; Pfaff, J.; Saykally, R. J. Velocity-Modulated Infrared Laser Spectroscopy of Molecular Ions: The ν_1 Band of HCO$^+$. *Phys. Rev. Lett.* **1983**, 50, 727−731.

(3) Stephenson, S. K.; Saykally, R. J. Terahertz Laser Velocity Modulation Spectroscopy of Ions. *J. Mol. Spectrosc.* **2005**, 231, 145−153.

(4) Gudeman, C. S.; Saykally, R. J. Velocity Modulation Infrared Laser Spectroscopy of Molecular Ions. *Annu. Rev. Phys. Chem.* **1984**, 35, 387−418.

(5) Farley, J. Theory of the Resonance Line-Shape in Velocity-Modulation Spectroscopy. *J. Chem. Phys.* **1991**, 95, 5590−5602.

(6) Amano, T. The ν_1 Fundamental Band of HCO$^+$ by Difference Frequency Laser Spectroscopy. *J. Chem. Phys.* **1983**, 79, 3595.

(7) Verbraak, H.; Ngai, A. K. Y.; Persijn, S. T.; Harren, F. J. M.; Linnartz, H. Mid-Infrared Continuous Wave Cavity Ring Down

10039

dx.doi.org/10.1021/jp400570m | *J. Phys. Chem. A* 2013, 117, 10034−10040

Spectroscopy of Molecular Ions Using an Optical Parametric Oscillator. *Chem. Phys. Lett.* **2007**, *442*, 145−149.

(8) Buhl, D.; Snyder, L. E. Unidentified Interstellar Microwave Line. *Nature* **1970**, *228*, 267−269.

(9) Klemperer, W. Carrier of the Interstellar 89.190 GHz Line. *Nature* **1970**, *227*, 1230−1230.

(10) Woods, R.; Dixon, T.; Saykally, R.; Szanto, P. Laboratory Microwave Spectrum of HCO⁺. *Phys. Rev. Lett.* **1975**, *35*, 1269−1272.

(11) Sanchez Contreras, C.; Sahai, R. Physical Structure of the Protoplanetary Nebula CRL 618. II. Interferometric Mapping of Millimeter-Wavelength HCN *J* = 1−0, HCO⁺ *J* = 1−0, and Continuum Emission. *Astrophys. J.* **2004**, *602*, 960−977.

(12) Purcell, C. R.; Balasubramanyam, R.; Burton, M. G.; Walsh, A. J.; Minier, V.; Hunt-Cunningham, M. R.; Kedziora-Chudczer, L. L.; Longmore, S. N.; Hill, T.; Bains, I.; et al. A CH₃CN and HCO⁺ Survey Towards Southern Methanol Masers Associated with Star Formation. *Mon. Not. R. Astron. Soc.* **2006**, *367*, 553−576.

(13) Liszt, H.; Lucas, R. mm-wave HCO⁺, HCN and CO Absorption Toward NGC-1052. *Astron. Astrophys.* **2004**, *428*, 445−450.

(14) Milam, S. N.; Savage, C.; Ziurys, L. M.; Wyckoff, S. HCO⁺ Observations Toward Comet Hale-Bopp (C/1995 O1): Ion−Molecule Chemistry and Evidence for a Volatile Secondary Source. *Astrophys. J.* **2004**, *615*, 1054−1062.

(15) Cazzoli, G.; Cludi, L.; Buffa, G.; Puzzarini, C. Precise THz Measurements of HCO⁺, N₂H⁺, and CF⁺ for Astronomical Observations. *Astrophys. J., Suppl. Ser.* **2012**, *203*, 11.

(16) Lattanzi, V.; Walters, A.; Drouin, B. J.; Pearson, J. C. Rotational Spectrum of the Formyl Cation, HCO⁺, to 1.2 THz. *Astrophys. J.* **2007**, *662*, 771−778.

(17) Crabtree, K. N.; Hodges, J. N.; Siller, B. M.; Perry, A. J.; Kelly, J. E.; Jenkins, P. A., II; McCall, B. J. Sub-Doppler Mid-Infrared Spectroscopy of Molecular Ions. *Chem. Phys. Lett.* **2012**, *551*, 1−6.

(18) Mills, A. A.; Siller, B. M.; McCall, B. J. Precision Cavity Enhanced Velocity Modulation Spectroscopy. *Chem. Phys. Lett.* **2010**, *501*, 1−5.

(19) Donley, E. A.; Heavner, T. P.; Levi, F.; Tataw, M. O.; Jefferts, S. R. Double-Pass Acousto-Optic Modulator System. *Rev. Sci. Instrum.* **2005**, *76*, 063112.

(20) Siller, B. M.; Porambo, M. W.; Mills, A. A.; McCall, B. J. Noise Immune Cavity Enhanced Optical Heterodyne Velocity Modulation Spectroscopy. *Opt. Express* **2011**, *19*, 24822−24827.

(21) Hirota, E.; Endo, Y. Microwave Spectroscopy of HCO⁺ and DCO⁺ in Excited Vibrational States. *J. Mol. Spectrosc.* **1988**, *127*, 527−534.

(22) Blake, G. A.; Laughlin, K. B.; Cohen, R. C.; Busarow, K. L.; Saykally, R. J. Laboratory Measurement of the Pure Rotational Spectrum of Vibrationally Excited HCO⁺ (ν_2 = 1) by Far-Infrared Laser Sideband Spectroscopy. *Astrophys. J.* **1987**, *316*, L45−L48.

■ NOTE ADDED AFTER ASAP PUBLICATION

This article was published ASAP on July 3, 2013. After this paper was finalized, comb-calibrated sub-Doppler spectra were obtained for the P(5) and R(3) transitions, and the line centers were 4.1(6) and 3.7(8) MHz, respectively, lower than the values in Table 1 from our single-pass measurements. This evidently systematic offset is likely due to an asymmetry in the ion drift velocity in our AC plasma, and does not affect the indirect rotational transitions reported here as the offset is removed by subtraction. Since the observed Lamb dips probe only the zero-velocity ion population, we expect their frequencies to be independent of any plasma asymmetry. The corrected version was published ASAP on July 10, 2013.

High-precision and high-accuracy rovibrational spectroscopy of molecular ions

James N. Hodges, Adam J. Perry, Paul A. Jenkins, Brian M. Siller, and Benjamin J. McCall

Additional information on J. Chem. Phys.

High-precision and high-accuracy rovibrational spectroscopy of molecular ions

James N. Hodges,[1] Adam J. Perry,[1] Paul A. Jenkins II,[1] Brian M. Siller,[1,a)] and Benjamin J. McCall[1,2,b)]

[1]*Department of Chemistry, University of Illinois, Urbana, Illinois 61801, USA*
[2]*Departments of Astronomy and Physics, University of Illinois, Urbana, Illinois 61801, USA*

We present a versatile new instrument capable of measuring rovibrational transition frequencies of molecular ions with sub-MHz accuracy and precision. A liquid-nitrogen cooled positive column discharge cell, which can produce large column densities of a wide variety of molecular ions, is probed with sub-Doppler spectroscopy enabled by a high-power optical parametric oscillator locked to a moderate finesse external cavity. Frequency modulation (heterodyne) spectroscopy is employed to reduce intensity fluctuations due to the cavity lock, and velocity modulation spectroscopy permits ion-neutral discrimination. The relatively narrow Lamb dips are precisely and accurately calibrated using an optical frequency comb. This method is completely general as it relies on the direct measurement of absorption or dispersion of rovibrational transitions. We expect that this new approach will open up many new possibilities: from providing new benchmarks for state-of-the-art *ab initio* calculations to supporting astronomical observations to helping assign congested spectra by combination differences. Herein, we describe the instrument in detail and demonstrate its performance by measuring ten R-branch transitions in the ν_2 band of H_3^+, two transitions in the ν_1 band of HCO^+, and the first sub-Doppler transition of CH_5^+. © *2013 AIP Publishing LLC*. [http://dx.doi.org/10.1063/1.4825251]

I. INTRODUCTION

In the 30 years since its discovery,[1] velocity modulation spectroscopy (VMS) in a positive column discharge has been a tremendously successful method for performing direct absorption spectroscopy of molecular ions. The positive column offers a remarkably rich chemical environment suitable for the production of a wide variety of ions with a high column density.[2]

Traditional VMS has been limited in its frequency precision by broad Doppler-limited linewidths, coupled with modest signal-to-noise ratios, and the uncertainties in line center determinations are typically 30-90 MHz.[3,4] The Doppler limit was overcome by our group in 2010 by placing the discharge cell in an external cavity, in an approach called cavity enhanced VMS.[5,6] The high intracavity power enabled saturation spectroscopy, and the resulting Lamb dips enabled the precision to be improved to ∼3 MHz in the near-infrared. The later incorporation of frequency modulation, or heterodyne, spectroscopy improved the signal-to-noise ratio and further improved the precision.[7] This approach, based on the pioneering NICE-OHMS technique,[8] was dubbed NICE-OHVMS, or Noise Immune Cavity Enhanced Optical Heterodyne Velocity Modulation Spectroscopy. This technique was later extended into the mid-infrared, using an optical parametric oscillator, by Crabtree *et al.*[9]

The accuracy of VMS has also been limited by the method of frequency calibration. Typically, VMS experiments relied on a combination of relative calibration using marker etalons and absolute calibration using Doppler-limited reference gas transitions, which were themselves often only known to ∼30 MHz accuracy. The advent of optical frequency combs has revolutionized the accuracy of molecular spectroscopy, making sub-MHz frequency measurements almost routine. Our near-infrared NICE-OHVMS work on N_2^+ used a frequency comb to achieve an accuracy of ∼300 kHz.[7] In recent work without an external cavity, we have demonstrated that it is possible to extend comb-calibrated spectroscopy to the mid-infrared, to infer pure-rotational transitions of molecular ions such as HCO^+ using combination differences with sub-MHz accuracy.[10]

In this paper, we present the combination of sub-Doppler spectroscopy using mid-infrared NICE-OHVMS[9] with optical frequency comb calibration[10] to yield a versatile method for molecular ion spectroscopy with both high precision and high accuracy. We demonstrate and characterize the effectiveness of this method through spectroscopy of H_3^+, HCO^+, and CH_5^+.

H_3^+ is a natural first target for our spectrometer. As the simplest polyatomic molecule, it has become an important system for benchmarking the increasing accuracy of quantum calculations. Many of its rovibrational transitions have been predicted to within hundredths of a wavenumber by sophisticated calculations that include adiabatic, relativistic electron, and non-adiabatic corrections to the Born-Oppenheimer potential energy surface.[11] In many cases, this degree of precision is comparable to the experimental uncertainties, so more precise measurements will serve to motivate and benchmark ever more accurate calculations, which will require the
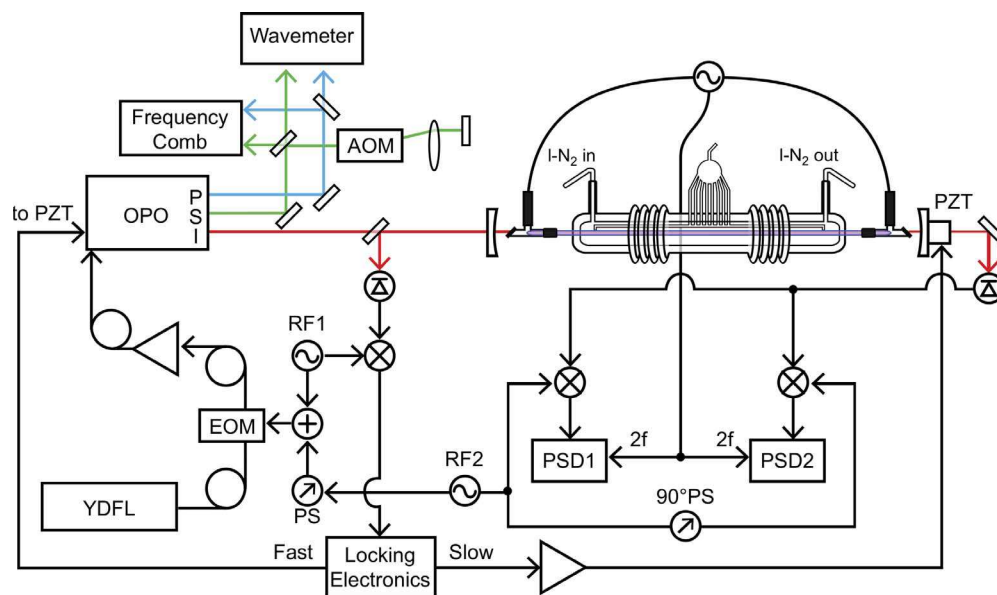
FIG. 1. Block diagram of the instrument. YDFL: Ytterbium Doped Fiber Laser; EOM: Electro-Optic Modulator; OPO: Optical Parametric Oscillator; P,S,I: Pump(Blue), Signal(Green), Idler(Red); AOM: Acousto-Optic Modulator; PZT: Piezo-electric Transducer; PS: Phase Shifter; RF: Radio-Frequency source; and PSD: Phase Sensitive Detector.

inclusion of quantum electrodynamic effects as has already been done with diatomics[12] and H_2O.[13]

In addition to its fundamental interest, H_3^+ is also an important molecule in astrochemistry due to its abundance in both dense[14] and diffuse[15] interstellar clouds, as well as in the atmospheres of large gas giants such as Jupiter.[16] Of particular relevance to the present work, the Doppler shifts of H_3^+ rovibrational transitions have been successfully used to determine the velocity of Jovian auroral winds,[17] but the accuracy of those determinations is limited by the uncertainties in the laboratory transition frequencies.

Our second target, HCO^+, was recently used[10] to demonstrate the feasibility of performing "indirect" pure-rotational spectroscopy by calculating combination differences of high-precision rovibrational frequencies. Due to degradation of our cavity mirrors in that work, we were restricted to performing single-pass heterodyne spectroscopy. Here, we revisit HCO^+ with an improved set of cavity mirrors, and we find that the single-pass measurements suffered a slight (~4 MHz) but systematic offset due to an asymmetry in the AC plasma. This highlights the advantage of using Lamb dips in a bidirectional cavity for line center determination, as they are located symmetrically around the zero-velocity component of the ions and are not shifted by plasma asymmetries.

Our final target, CH_5^+, is an enigmatic ion whose high-resolution infrared spectrum in the C–H stretching region remains completely unassigned nearly 15 years since it was first reported.[3] It has been suggested[18] that one possible way of assigning the spectrum would be to search for four-line combination differences, which would identify energy level separations. However, the high line density results in many "false positives" at the current precision of the line center measurements. Here we report the first sub-Doppler spectrum of CH_5^+, which improves on the precision of the initial detection[3] by more than two orders of magnitude.

II. EXPERIMENTAL DESCRIPTION

A block diagram of the instrument is presented in Figure 1. A ytterbium doped fiber laser (Koheras Adjustik Y-10) is coupled into a fiber electro-optic modulator (EOSPACE PM-0K5-00-PFU-PFU-106-S), where Pound Drever Hall (PDH) locking side bands (~4 MHz) and heterodyne sidebands (~79 MHz, equal to the free spectral range of our external cavity) are imprinted onto the laser. After modulation, the light is amplified by a 10 W fiber amplifier (IPG Photonics YAR-10 K-1064-LP-SF) and is used to pump a singly resonant optical parametric oscillator (OPO; Aculight Argos 2400 SF). The idler, tunable from 3.2 to 3.9 μm, is coupled into a ~190 cm external cavity composed of two dielectric mirrors (Rocky Mountain Instruments, custom) on silicon substrates with 1 m radius of curvature. For the H_3^+ measurements, the mirrors used were nominally 99.7% reflective between 3.0 and 3.4 μm but suffered high losses at higher frequencies because of water adsorbed in the hygroscopic coating. The measurements of HCO^+ and CH_5^+ have utilized a new set of mirrors, nominally 99% reflective between 3.0 and 3.4 μm, which were specially coated with a protective layer to prevent the uptake of water. Additionally, the newer mirrors are kept under a flow of dry nitrogen at all times.

The cavity and the idler are locked to maintain resonance by using a detector (Boston Electronics Vigo PVM-10.6-1x1) to monitor the back reflection from the front cavity mirror. The signal from that detector is demodulated with a mixer that is referenced to the PDH locking sideband frequency. The output of that mixer is processed by a lock box, and slow corrections (<100 Hz) are sent to a piezo on which one of the cavity mirrors is mounted, to keep the cavity locked onto the idler on slow timescales. Faster corrections (0.1–10 kHz) are sent to a piezo that controls the length of the OPO cavity, thus making small corrections to the frequency of the signal and the idler

to keep the idler resonant with the cavity on fast timescales. Based on the observed magnitude of this error signal, there is an extra ∼500 kHz of random noise imposed upon the signal frequency (and therefore also upon the idler frequency) due to the locking of the idler frequency to the external cavity.

Within the external cavity is a liquid nitrogen cooled positive column discharge cell (Black Widow), which was used extensively for VMS in the Oka group at the University of Chicago. An arbitrary waveform generator (Agilent 33120A) creates a sine wave, which is amplified (Techron 7780) and sent to a step-up transformer to drive the plasma. The AC voltage configuration of the plasma modulates the velocity of the ions at a frequency of 40 kHz. Optimal signals for H_3^+ have been observed at 200 mTorr of cell pressure and 170 mA of current. For HCO^+, we used a mixture of 17:3 H_2:CO at a total pressure of 200 mTorr, and a plasma current of 115 mA. CH_5^+ was observed using a 24:1 mixture of H_2:CH_4 at 250 mTorr and the lowest possible current the discharge could maintain, typically ∼110 mA.

The idler radiation from the OPO is coupled through the discharge cell by CaF_2 windows that are aligned at Brewster's angle. The transmitted light through the cavity is detected and demodulated first at the heterodyne frequency of ∼79 MHz by a pair of mixers that are 90° out of phase with each other. The outputs from these mixers are further demodulated via lock-in amplifiers referenced to 80 kHz, twice the plasma modulation frequency. The detection scheme results in four data channels: in-phase and quadrature detection for each of the two mixers. Previously, we have estimated the sensitivity of our spectrometer in the lowest noise channel to be 9.8×10^{-10} cm^{-1} Hz$^{-1/2}$.[9]

Frequency calibration of the idler is accomplished by simultaneously measuring the frequency of the pump and signal beams using an optical frequency comb (Menlo Systems FC-1500, with 100 MHz repetition rate) and determining the difference between them. First, the carrier envelope offset of the comb is tuned to ∼20 MHz to be measured by a frequency counter, although this is not strictly necessary for measuring the idler frequency. The repetition rate of the comb is tuned such that the beat frequency of the signal with the comb is between 25 and 35 MHz, the range of the internal bandpass of the frequency counter used for the signal. Next, the pump is tuned so that its beat with the comb is ∼20 MHz. Then the signs of the beats and carrier envelope offset are determined. The pump is then offset locked to the comb using a frequency to voltage converter to generate an error signal. A wavemeter (Burleigh WA-1500, 0.2 ppm accuracy) then sequentially measures the pump and signal wavelengths to determine the mode numbers of the comb teeth that are closest to these two frequencies.

For spectroscopy, the idler is tuned by changing the repetition rate of the comb. The pump is dragged along with the comb, since it is offset-locked to the comb, but the signal remains relatively constant (aside from slow drift due to thermal variations of the OPO cavity). Without any correction, this would quickly lead to the signal beat with the comb moving out of the bandpass of our frequency counter. Therefore, we double-pass the signal through an acousto-optic modulator (Brimrose IPF-200-80-1600) before sending it to the beat

detection unit of the comb. The AOM frequency is adjusted with a feed forward as the comb repetition rate is changed, in order to keep the signal beat within the bandpass. The diffraction efficiency of the AOM allows it to be tuned between 150 and 210 MHz, leading to a shift of the signal frequency by 300 to 420 MHz. When the frequency limit of the AOM is reached, the frequency is increased or decreased by 50 MHz, which corresponds to a 100 MHz change in signal frequency, and the recorded mode number for the signal is incremented or decremented appropriately. The known frequency shift induced by the AOM is subtracted from the signal frequency determined by the comb before the latter is subtracted from the pump frequency to determine the idler frequency.

Data points are acquired with a separation in time of 1.5 s, which is ample time for the lock-in amplifiers to integrate (with a time constant of 300 ms) and the frequency counters to update (at a rate of 1 Hz). These steps are taken to minimize any line dragging by delayed detection. Scanning is performed both from low to high frequency and also from high to low frequency in order to remove any systematic errors caused by line dragging.

The use of the repetition rate for tuning limits the width of a single scan window to ∼900 MHz. In practice, this means that entire Doppler profiles of light ions such as H_3^+ cannot be measured in a single scan. In such cases, preliminary scans are taken without the frequency comb (by directly scanning the voltage on the fiber laser) over a wide range, and then the sub-Doppler features are scanned with the comb. For the heavier ions HCO^+ and CH_5^+, it is possible to record the full Doppler profile within a single scan.

III. RESULTS AND DISCUSSION

A. Lineshape fitting and uncertainty determination

The symmetry of the overall NICE-OHVMS lineshape is odd in both absorption and dispersion. For high precision line center determination, the most important part of the line is the Lamb dips that are evenly spaced about the transition's center frequency. The Lamb dips are a result of the forward- and counter-propagating beam sampling single velocity components on opposite sides of the Doppler profile. The frequency modulation effectively produces three lasers spaced by the modulation frequency: a carrier and two sidebands, one in phase with the carrier, and the other 180° out of phase. Assuming that both the carrier and sidebands are intense enough to contribute to saturation, and that the modulation index is low enough to avoid contributions of higher-order sidebands, there exist four separate Lamb dips that can be detected in absorption, spaced evenly in half integer multiples of the heterodyne frequency about the linecenter. In dispersion, there is also a fifth Lamb dip at the linecenter. In this work, detection was performed at a blended phase that provided the optimal signal-to-noise in all four channels, so the observed Lamb dips are from neither purely absorption nor purely dispersion. However, these individual Lamb dips are not resolved in this experiment because half of the heterodyne frequency is smaller than the full-width at half-maximum of the individual Lamb dips; thus we observe a blend of the five Lamb dips. For
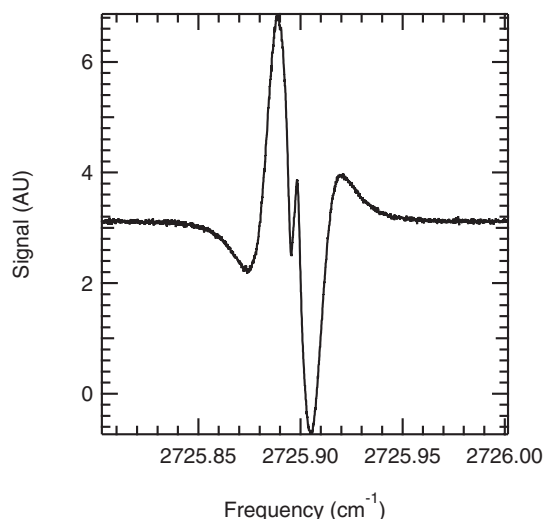
FIG. 2. A representative scan of the R(1,0) transition of H_3^+, illustrating the odd symmetry of the Doppler broadened lineshape. The sharp central feature is composed of five blended Lamb dips. This spectrum was only calibrated with a wavemeter, limiting its accuracy to 70 MHz.

The derivation of the sub-Doppler lineshape and the fits function have been presented in an earlier paper.[9] However, for clarity, the fitting procedure will be reviewed in brief. The fit is a nonlinear least squares fit using an equation that models the Lamb dips and fits the central portion of the Doppler profile with a cubic polynomial. The four individual channels are fit simultaneously with some shared parameters such as the linecenter to make the four fits self-consistent. The equation describing the Lamb dip shape is a sum of absorption and dispersion components, χ_{abs} and χ_{disp}, respectively,

$$\chi_{tot}(\nu_d) = \chi_{abs}(\nu_d) \sin \theta_h + \chi_{disp}(\nu_d) \cos \theta_h, \quad (1)$$

$$\chi_{abs}(\nu_d) = A_1 \left[\chi \left(\nu_d - \frac{f_h}{2} \right) - \chi \left(\nu_d + \frac{f_h}{2} \right) \right]$$
$$+ A_2 [\chi(\nu_d - f_h) - \chi(\nu_d + f_h)], \quad (2)$$

$$\chi_{disp}(\nu_d) = -A_0 \chi(\nu_d) + A_1 \left[\chi \left(\nu_d - \frac{f_h}{2} \right) + \chi \left(\nu_d + \frac{f_h}{2} \right) \right]$$
$$+ A_2 [\chi(\nu_d - f_h) + \chi(\nu_d + f_h)]. \quad (3)$$

purposes of illustration, the full profile from a single detection channel (not comb calibrated) of an H_3^+ transition is shown in Figure 2, and an example of the fit to the blended Lamb dips in all four simultaneously acquired detection channels is shown in Figure 3.

Here A_n denotes the amplitude of the Lamb dip where n is the order, i.e., A_0 is the amplitude of the central Lamb dip, A_1 is the amplitude of the first set of Lamb dips out from the linecenter and so forth. The frequency detuning from the linecenter is given by ν_d, f_h is the heterodyne frequency, and
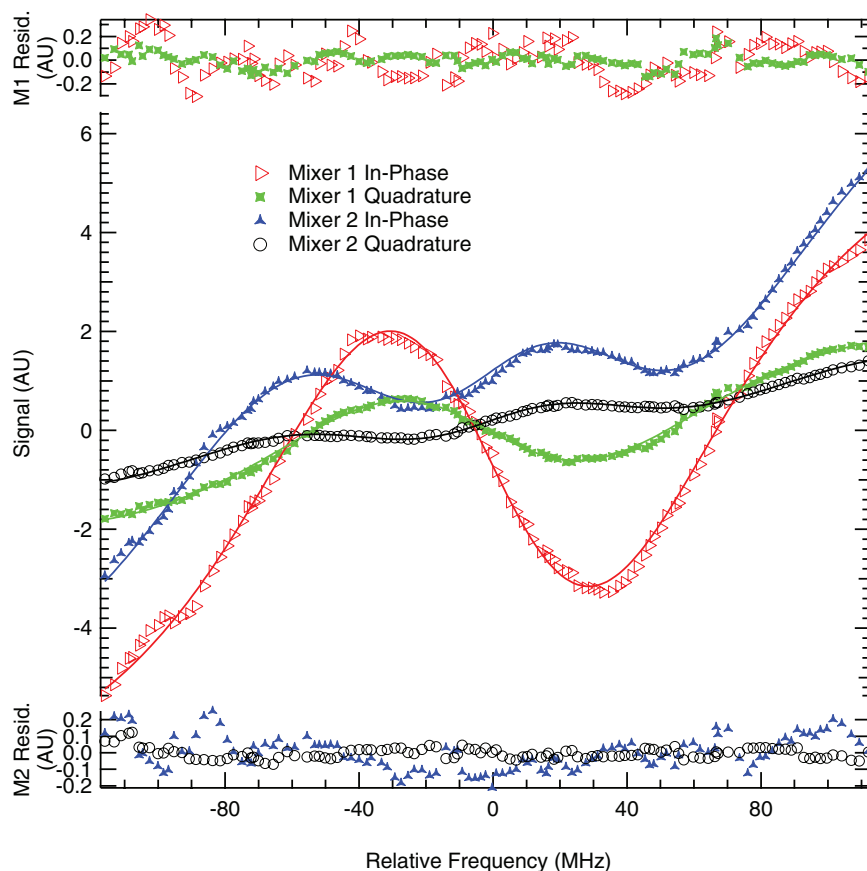

FIG. 3. Enlarged view of the Lamb dips in the R(2,2)^l transition of H_3^+, along with fits to the functional form presented in an earlier paper.[9] The four channels (two from the phase sensitive detector associated with each mixer) are presented in the center of the panel, with the residuals plotted above and below the fit. The data are shown as markers and the fits as solid lines.

θ_h is the heterodyne detection angle. The χ with no subscript is the lineshape for an individual Lamb dip, which depends on the linewdith though it is not explicitly shown in the above equations. In the case of absorption, it takes the form of a linear combination of a Lorentzian and a Gaussian. In the case of dispersion, the Lamb dips are modeled by the result of the Kramers-Krönig relation applied to the linear combination used in absorption. For more information about the fitting, we refer the reader to Crabtree *et al.*[9] Due to the blended nature of the Lamb dips, we were concerned about the potential for small changes in parameters significantly affecting the determination of the linecenter. The only part of the lineshape function that does not rely on a physical model is the fit to the central portion of the Doppler profile. Changing any of those values might make a detectable difference linecenter frequency. To simulate this, we increased the slope of the linear term in all four channels of a scan of the H_3^+ R(1,0) transition by 3 times the uncertainty in the slope returned by the original fit; this corresponds to ~3% of the total slope. The cubic term was held at zero to prevent it from compensating for the change in the linear term. This increased slope was held fixed as the data were re-fit. This simulation was repeated, decreasing the slope rather than increasing it. The linear term is the largest contributor to the polynomial part of the fit and adjusting it by 3σ in either direction only produced an error of ~27 kHz (+28 kHz for $+3\sigma$, −26 kHz for -3σ), which is well below the precision of the linecenter derived from the fit (~80 kHz) or the statistical error resulting from scan-to-scan variability (~240 kHz).

Each transition was scanned at least five times, and in some cases many more times. The linecenters determined from the fit to each scan were averaged and are reported below as the experimentally determined linecenter. The standard deviation of the individual linecenter measurements was determined and is reported to illustrate the spread of the distribution for linecenters. The standard error, also known as the standard deviation of the mean, which is simply the standard deviation divided by the square root of the number of samples, is also reported as our best estimate of the uncertainty of the average linecenter, under the assumption that the measurements are normally distributed.

B. H_3^+ spectroscopy

Our results for ten transitions of the R-branch of the ν_2 band of H_3^+ are reported in Table I. Our results are compared with those from the best available Doppler-limited spectra from the literature. In most cases, these are from the Ph.D. thesis of Wu[19] in the group of Shy, using frequency comb calibration; two transitions not observed by Wu were measured in the FTIR spectra of McKellar and Watson,[20] and the R(4,4)^l transition has not been reported since Oka's work in 1981.[21] In all cases, there is good agreement with the previous values, given the uncertainties of the latter, and in all but two cases the standard error of our measurements is sub-MHz.

With such high precision transition frequency data available, it is interesting to compare the determined transition frequencies to those previously determined to assess the quality

TABLE I. Determined line center frequencies, standard deviations, and standard errors of transitions in the ν_2 band of H_3^+. Previous values are given with the source as a footnote. The differences between the measured frequency and the previous best frequency are also reported. All values are in MHz.

Transition	Freq.	St. Dev.	St. Err.	Prev. Value	Diff.
R(1,1)^l	80687424.25	1.65	0.62	80687432(10)[a]	− 7.75
R(1,0)	81720377.29	0.86	0.23	81720370(10)[a]	7.29
R(1,1)^u	81730020.44	0.84	0.38	81730026(20)[a]	− 5.56
R(2,2)^l	82804769.99	0.70	0.31	82804764(10)[a]	5.99
R(2,1)^l	82908940.58	2.79	1.25	82908950(150)[b]	− 9.42
R(2,2)^u	84635537.25	1.21	0.54	84635542(10)[a]	− 4.75
R(2,1)^u	84724846.57	0.85	0.38	84724851(10)[a]	− 4.43
R(3,3)^l	84839013.46	0.88	0.39	84839025(10)[a]	− 11.54
R(3,2)^l	84907118.76	2.99	1.34	84907160(150)[b]	− 41.24
R(4,4)^l	86774648.52	1.28	0.39	86774570(300)[c]	78.52

[a]Reference 19.
[b]Reference 20.
[c]Reference 21.

of the older work. Especially noteworthy in this comparison is the high degree of accuracy of the FTIR work by McKellar and Watson.[20] As can be seen in Table II, their work is considerably more accurate than their stated uncertainty (150 MHz). Indeed, one of the weakest lines observed in their experiment, R(3,2)^l, is only ~40 MHz away from our determined linecenter.

There has been one other recently reported sub-Doppler measurement of the linecenter of the R(1,0) transition, from Shy's group.[22] They produce H_3^+ in an extended negative glow discharge at 30-80 mTorr and use an OPO in a strong pump, weak probe double pass configuration. Rather than scanning over the transition, calibrating each point, and fitting to determine the line center (as we have done), they instead lock their laser to the Lamb dip and use a frequency comb to measure the laser's frequency while locked. Their reported linecenter is 5.74 MHz lower than ours, a discrepancy which is far larger than the adopted uncertainties (~250 kHz in both cases). Subsequent measurements of other transitions in Shy's laboratory[23] also differ from our values, with discrepancies that vary in sign but are all of order 5 MHz.

TABLE II. A comparison to the FTIR values as determined by McKellar and Watson.[20] The error listed is the difference between our reported value and that determined by McKellar and Watson.

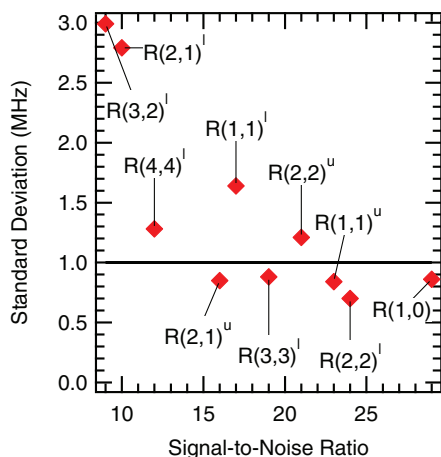| Transition	Error (MHz)
R(1,1)^l	− 5.75
R(1,0)	11.12
R(1,1)^u	19.65
R(2,2)^l	− 5.03
R(2,1)^l	− 12.42
R(2,2)^u	− 10.75
R(2,1)^u	− 9.43
R(3,3)^l	− 3.54
R(3,2)^l	− 41.24

FIG. 4. The standard deviation of the frequency measurements for each H_3^+ transition plotted against the average signal-to-noise ratio of the blended Lamb dip. The horizontal line at 1 MHz is drawn to indicate that the standard deviation is scattered about it for most transitions.
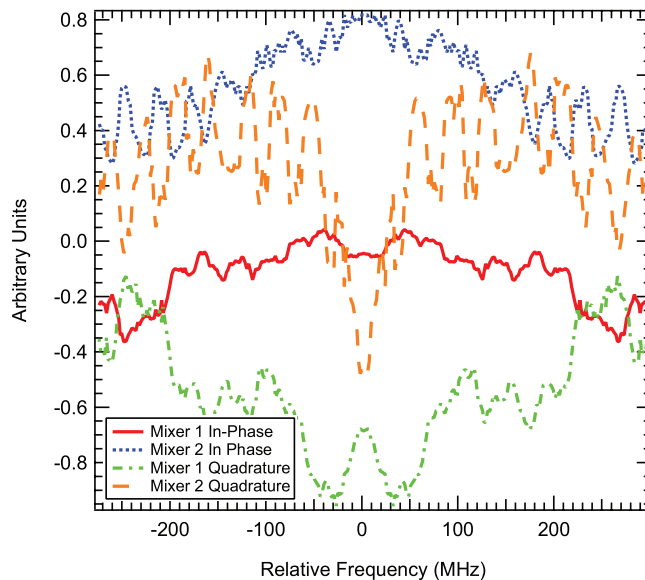

FIG. 5. A typical graph depicting the inversion residuals. It is evident that they are symmetric about the transition frequency, due to the process of additively imprinting the noise of one half of the line on the other. These data are used to calculate characteristic parameters of the asymmetry.

Because of these discrepancies, we have taken great care to characterize potential sources of systematic and random errors in our experiment, as described in Secs. III B 1–III B 4.

1. Effect of signal-to-noise ratio

The precision of the linecenters derived from the fits to our individual scans is typically a few hundred kHz, but can be as low as 70 kHz. Clearly, the fit precision is not the limiting factor in our measurements. To assess the effect of the signal-to-noise ratio of the Lamb dips on our linecenter measurements, the average signal-to-noise ratio of the blended Lamb dips for each transition is plotted against the standard deviation of its linecenter, as determined from several scans over each transition, in Figure 4.

All except the two weakest transitions are clustered near the horizontal line at 1 MHz; these two transitions have fits that are less well determined, which is the cause of the greater uncertainty in their linecenters. No gradual trend in the standard deviation as a function of signal-to-noise ratio is evident, indicating that there is some other dominant effect limiting the standard deviation for all but the weakest lines.

2. Effect of asymmetry

In Crabtree *et al.*,[9] the effect of asymmetry on the determined transition frequency was left as an unanswered question due to the fact that the accuracy was limited to ∼70 MHz by the wavemeter calibration. In that work, several simulated asymmetries were used to intentionally affect the ability to fit the lines, though no physical meaning or mechanism was used in the simulations. The largest magnitude effects were found to cause a few MHz shift in transition frequency, and this was interpreted as a firm upper limit on the potential effect of asymmetry.

With the inclusion of a frequency comb, the effect caused by asymmetry can now be better characterized. For this purpose, the R(1,0) transition was scanned many times on many different days to study the asymmetry. In all cases, the fit

residuals do not indicate any obvious asymmetry in the Lamb dips, which would have the largest effect in the determination of linecenters. Instead, the Doppler profiles clearly exhibit asymmetric lineshapes, and the amount and sign of this asymmetry changes over time and from scan to scan.

To quantify the amount of asymmetry (deviation from the expected odd symmetry) in each scan, we first trimmed each channel of a scan to an equal number of data points on each side of the line center, and shifted it by the y-offset determined from the fit. A copy of the data was made and then the frequency axis was inverted, mirroring the data across the linecenter. The original scan channels and mirrored scan channels were added together to create a graphical representation of the asymmetry (Figure 5), which we refer to as the inversion residuals.

From the inversion residuals, two parameters were determined. The first, the offset asymmetry parameter, was defined as the average value of all four channels. The average value from each individual channel was determined, then these four averages were averaged together. The offset asymmetry parameter was defined in this manner to capture the effect that each individual channel would have on the simultaneous least squares fit of all four channels. In the case of a perfectly symmetric line, the offset parameter would have a value of zero because the odd lineshape would cancel itself out. Negative values of the offset parameter indicate that the lower frequency (negative-going) lobe is stronger than the higher frequency lobe; whereas, positive values indicate stronger lobes on the high frequency side.

The second parameter, which we refer to as the high-low asymmetry parameter, represents the average difference between the maximum and minimum values for each of the four inversion residuals. The high-low parameter is intended to capture an imbalance in the shape of the line. Such an imbalance would manifest itself in the inversion residuals as a
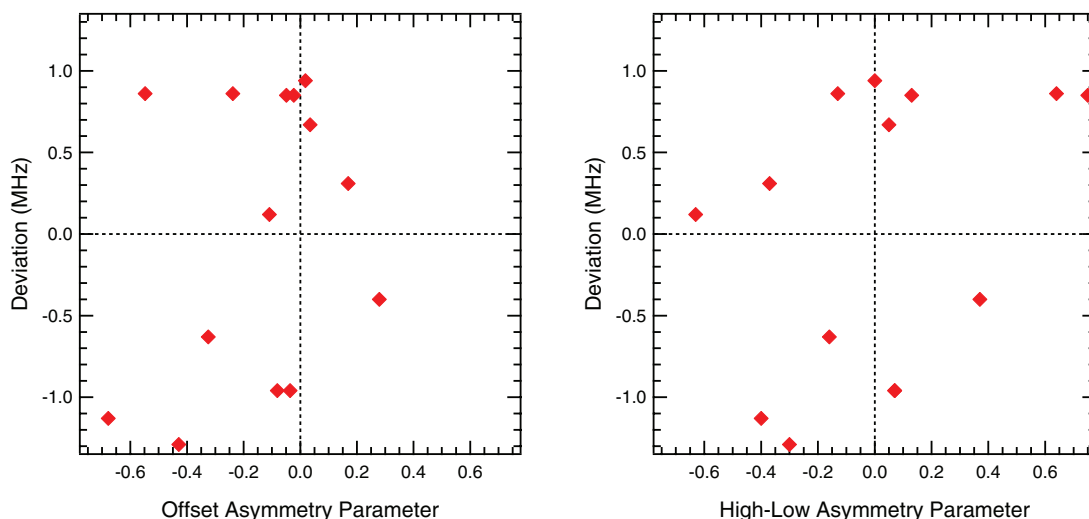
FIG. 6. The deviation of the linecenter of a given scan from the mean value versus the offset asymmetry parameter (left panel) and the high-low asymmetry parameter (right panel). The dotted lines shows the zero crossings to emphasize the insensitivity of the sign of the difference to the sign of the asymmetry parameter.

sloped or curved line. The magnitude of the slope is parameterized by differencing the maximum and minimum values of the residuals. These differences for each data channel are averaged just like the offset parameter. As above, the sign indicates which lobe was larger.

In Figure 6, the deviation of the linecenter of an individual scan from the mean of all R(1,0) scans is plotted against these two asymmetry parameters. The data show no clear trend, not even a consistent change in the sign of the deviation with the sign of the asymmetry parameter. Instead, the data are well scattered. If the scan-to-scan reproducibility in the linecenter of ∼1 MHz is due to the changing asymmetry, it must depend on the asymmetry in a way that is not captured by these particular metrics.

In any case, the fact that the amount and the sign of the asymmetry change from scan to scan strongly suggests that the asymmetry cannot cause a systematic shift in the linecenter in an ensemble of scans. Instead, we conclude that the impact of the asymmetry manifests itself as a random error, reflected in the magnitude of the standard deviation of the linecenter determinations.

3. Pressure shift

Given the difference in pressure between our experiment and Shy's, we decided to measure the linecenter of the R(1,0) transition at three different pressures to rule out the possibility of an unexpectedly large pressure shift. The results are displayed in Table III, and show the same linecenter (within uncertainties) from pressures between 200 and 500 mTorr. The largest pressure shift consistent with the data, determined from the lower bound of the 200 mTorr data (81 720 377.06 MHz) and the upper bound of the 500 mTorr data (81 720 377.86 MHz), would be 2.7 MHz/Torr at the 1σ level. This would mean our linecenter measured at 200 mTorr could be too high by at most 0.4 MHz from the value at 55 mTorr (the midpoint of Shy's range).

4. Comb calibration test

In order to rule out any unexpected problems with the calibration of our optical frequency comb, we wished to measure another transition that had been previously measured with high precision. Since there are no other ion transitions known to this level of accuracy in the mid-infrared, we pursued spectroscopy of neutral methane, which has comb calibrated lines in our spectral region that are known to high accuracy and precision.[24]

Obviously, NICE-OHVMS could not be performed because the instrument cannot modulate the velocity of a neutral molecule. Ordinary NICE-OHMS is challenging to perform with a fiber based EOM due to strong baseline drifts from residual amplitude modulation (RAM),[25,26] so an additional layer of modulation is necessary. The logical choice was wavelength modulation, but our pump laser must be locked to the comb and our use of an external cavity requires feedback to the OPO cavity length, which fixes the frequency of the signal. Therefore, the cavity was removed and the back reflection detector was used in a double pass configuration for wavelength modulated heterodyne spectroscopy.

Without the need to apply feedback to the OPO cavity length, this control could be used to apply a dither necessary to modulate the wavelength of the signal, and hence also the idler. A 1.4 kHz dither was applied to the cavity, and the lock-in amplifiers were referenced to three times the dither frequency. This allowed the system to be insensitive to the Doppler profile of the methane transition. The chosen target

TABLE III. Measured linecenters of the R(1,0) transition of H_3^+ at different pressures.

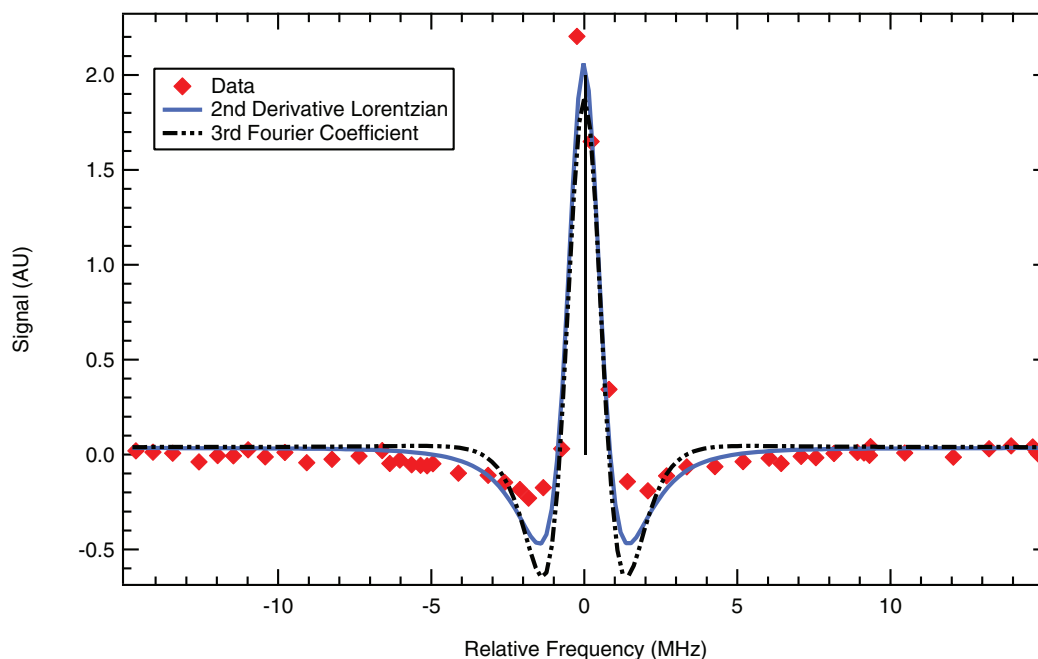| Pressure (mTorr)	Frequency (MHz)
200	81720377.29(23)
350	81720377.47(32)
500	81720377.44(42)

FIG. 7. The comb calibrated central Lamb dip of the $F_1^{(2)}$ component of the P(7) transition in the ν_3 band of methane. Fits to an analytical expression of the third Fourier coefficient for a wavelength modulated dispersion signal (dashed curve) and to the second derivative of a Lorentzian (solid curve) are shown. The black line is the linecenter determined by Takahata *et al.*[24]

was the $F_1^{(2)}$ component of the P(7) transition in the ν_3 band, which has been reported to kHz precision.[24] A few mTorr of methane was leaked into the discharge cell, and the central Lamb dip, which corresponds only to dispersion, was recorded.

The result of our methane spectroscopy is shown in Figure 7. We fit the data to both the third Fourier coefficient for a Lorentzian dispersion lineshape[27] and a simple second derivative of a Lorentzian. While neither fit perfectly reproduces the observed lineshape, the derived linecenters compare very favorably with the previous work of Takahata *et al.*[24] The linecenter as determined by the second derivative fit is 5 ± 22 kHz less than Takahata's, and that from the third Fourier coefficient fit was 10 ± 30 kHz greater than Takahata's. Even by the roughest approximation of simply picking the highest recorded point and calling it the line center, the error is only 222 kHz. Therefore, we conclude that our frequency comb system is working well, and is not the limiting source of error in our ion measurements.

C. HCO+ spectroscopy

While there are no molecular ion transitions in the mid-infrared previously measured with sub-MHz accuracy, there are ions (such as HCO+) for which pure rotational transitions are known with such accuracy. By measuring multiple rovibrational transitions and using combination differences, we can compare the results with observed rotational transitions as yet another check on the accuracy of our ion transition measurements.

We have recently performed such "indirect rotational spectroscopy" using Doppler-limited spectra of HCO+ with comb calibration.[10] Ultimately, we expect this approach to be a useful tool for inferring rotational spectra that have not been directly measured, in order to support astronomical observations with far-infrared/THz instruments such as SOFIA and ALMA. Here, we simply extend our previous work on HCO+ to demonstrate the accuracy of our sub-Doppler NICE-OHVMS spectra.

The P(5) and R(3) lines from the ν_1 band of HCO+ were measured (see Figure 8) in order to determine the energy level separation between $J = 5$ and $J = 3$ in the ground vibrational state. The two transitions were measured multiple times to determine their linecenters, which were 92 145 080.8(4) MHz for P(5) and 92 947 717.3(5) MHz for R(3). The difference between these frequencies, 802 636.5(7) MHz, agrees within its uncertainty with the sum of the $J = 3 \rightarrow 4$ and $J = 4 \rightarrow 5$ pure rotational transitions observed by Cazzoli *et al.*,[28] 356 734.2230(15) + 445 902.8721(15) = 802 637.0951(21) MHz. The excellent agreement of this combination difference strongly suggests that our experiment does not suffer from any systematic errors that differ from one line to the next, beyond those at the sub-MHz level that result from scan-to-scan variations.

It is interesting to note that the P(5) and R(3) frequencies determined from the Lamb dips are both $\sim$4 MHz lower than those determined from our earlier Doppler-limited, single-pass measurements.[10] This difference is evidently due to an asymmetry in the drift velocity of the ions on the two half-cycles of the AC discharge; such an asymmetry results in a net Doppler shift in the single-pass measurements, but the present measurements are insensitive to this effect due to the bi-directional nature of the cavity and the fact that the Lamb dips are located symmetrically about the zero-velocity component.
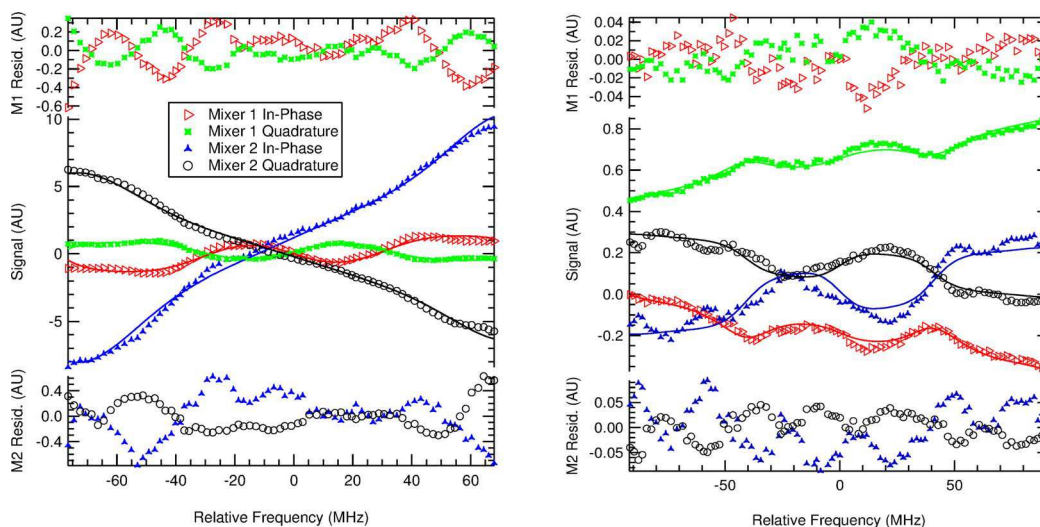
FIG. 8. Results from fitting the Lamb dips from the P(5) transition (left) and R(3) transition (right) of HCO$^+$. The four channels are presented with residuals from each mixer plotted above and below the fit. The data are shown as markers and the fits as solid lines.

D. CH$_5^+$ spectroscopy

An important future application of this technique will be high-precision and high-accuracy spectroscopy of highly congested spectra, such as that of CH$_5^+$. The infrared spectrum of this ion was first reported by the Oka group in 1999,[3] and consisted of about 900 spectral lines between 2770 and 3150 cm^{-1}, with no discernable patterns. The spectrum is complicated by the fact that CH$_5^+$ does not have a single equilibrium structure, but can sample all 5! = 120 equivalent minima of C$_s$ symmetry on its potential energy surface, as well as the C$_s$ and C$_{2v}$ saddle points that interconnect them. Many important theoretical studies (see, e.g., Refs. 29–35) have been undertaken since the publication of Oka's spectrum, and low-resolution spectra have been reported covering different frequency ranges[36] and temperatures.[31] Despite nearly 15 years of effort since the Oka group's first report, the community seems to be no closer to an assignment of Oka's spectrum.

One possible way forward is to search for four-line combination differences in the spectrum, that is, to look for two pairs of transitions with the same combination difference. This would represent an experimental measure of the separation between two rotational energy levels. If spectra with reliable intensities could be obtained at different temperatures, it may be possible to begin assembling an energy level diagram. Comparison between such experimentally determined energy levels and those predicted by sophisticated theoretical techniques might eventually lead to an assignment. However, the frequency uncertainties in the Oka group spectrum range from 90 to 180 MHz, as their measurements were limited by their Doppler linewidth, relatively low signal-to-noise ratio, and traditional frequency calibration techniques (reference gases). Given the line density, there are almost innumerable pairs of transitions whose combination differences agree within this level of uncertainty, and the vast majority of those are accidental rather than true four-line combination differences.

Progress on this front will necessitate remeasurements of CH$_5^+$ transitions with considerably higher accuracy and preci-

sion. The Schlemmer group recently made the first report of a high-resolution spectrum since Oka's, using a cryogenically cooled ion trap and laser-induced reaction spectroscopy.[37] With their smaller Doppler linewidth ($\sim$70 MHz at 20 K) and frequency comb calibration, they determined the central frequency of a CH$_5^+$ transition at 2932.998460 cm^{-1} to within $\sim$200 kHz. An alternative approach, which we are pursuing, is to obtain sub-Doppler spectra in a positive column discharge.

Our experiment uses the same discharge cell that was used for the first report of the CH$_5^+$ spectrum. We are attempting to reproduce the plasma conditions as closely as possible, but the CH$_5^+$ signal is exquisitely sensitive to the exact discharge conditions and we are still in the process of optimizing the system. Nevertheless, we have obtained several comb-calibrated scans of the transition Oka's group reported at 2898.008 cm^{-1}, with a signal-to-noise ratio that is somewhat higher than that of the Oka group. Given our $\sim$10-fold longer effective pathlength (from the cavity enhancement) and the fact that our noise level should be lower than Oka's (because of the frequency modulation), we suspect that further tuning of plasma conditions should lead to significantly stronger signals.

The average of five spectra of this transition is displayed in Figure 9, and represents the first sub-Doppler spectrum of CH$_5^+$. A fit to the averaged spectrum yields a linecenter of 86 880 178.469(126) MHz; the precision of this fit is more than two orders of magnitude lower than the $\sim$90 MHz uncertainty from the Oka group's measurements. The Schlemmer group has independently measured a CH$_5^+$ line centered at 86 880 178.22(63) MHz.[38] This transition is only $\sim$240 kHz different from our measurement, which agrees with our transition frequency within 1σ of their uncertainty and 2σ of our uncertainty. This provides independent confirmation of the accuracy of our technique. The weakness of the CH$_5^+$ Lamb dip, compared to those seen in H$_3^+$ and HCO$^+$, is likely the result of the lower transition dipole moment of CH$_5^+$. Although we are not aware of any predictions for the transition dipole moment, the MULTIMODE calculations of Huang *et al.*[31] show
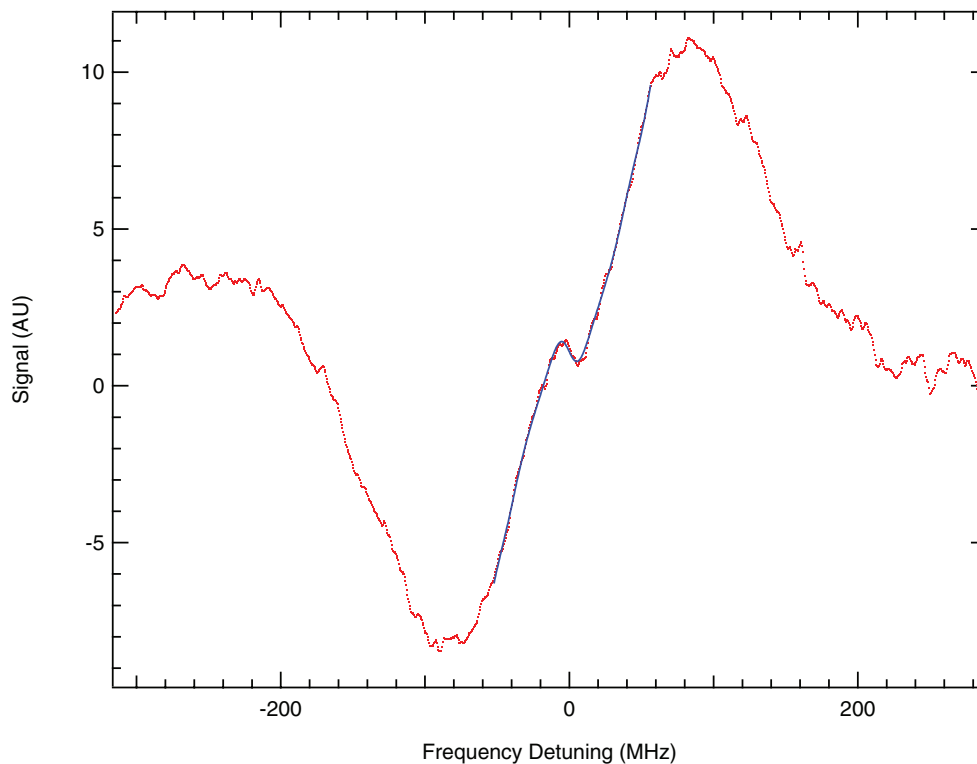
FIG. 9. Comb-calibrated NICE-OHVMS spectrum of Oka's "2898.008 cm^{-1}" transition of CH$_5^+$. The data are shown as red dots and the fit to the Lamb dip is shown as a blue line.

an integrated band intensity of ∼50 km/mol, which is considerably lower than the calculated value of 227 km/mol[39] for HCO$^+$.

In the future, we hope to increase the Lamb dip depth by increasing the power injected into our cavity and/or by obtaining mirrors with higher reflectivity. Even if this is not effective, we expect to be able to improve the signal-to-noise ratio on the Lamb dip by further optimization of the plasma conditions and by reducing technical noise sources in our spectrometer.

IV. CONCLUSIONS

We have demonstrated the first instrument capable of routine sub-Doppler spectroscopy of a wide variety of molecular ions, offering both high precision from optical saturation and high accuracy from optical frequency comb calibration. Using this instrument, ten lines of the doubly degenerate ν_2 band of H$_3^+$ have been measured, eight of which have sub-MHz uncertainties. Two lines from the ν_1 band of HCO$^+$ have also been measured with similar uncertainties, and their combination difference is in excellent agreement with pure rotational spectroscopy. The first sub-Doppler spectrum of CH$_5^+$ has also been recorded with sub-MHz precision, a substantial improvement over the ∼90 MHz uncertainty of the initial detection in the Oka group.[3]

Because our measurements of H$_3^+$ transitions disagree with those reported by Shy's group[22,23] by ∼5 MHz, we have conducted an extensive analysis of potential sources of experimental error in our instrument. The limiting factor in our

frequency determinations appears to be scan-to-scan variability that is not yet understood, but results in a standard deviation among individual scans of ∼1 MHz. The standard error of a set of scans can be reduced to ∼250 kHz by performing multiple scans. The scan-to-scan variability may be due to varying asymmetry of the Doppler-broadened lineshape, but our attempts to find correlations between the center frequency deviations and measures of the asymmetry have not been successful. All indications are that our determined standard errors accurately capture the random errors in our measurements. This conclusion is further supported by the excellent combination difference between the HCO$^+$ transitions we measured. We have also excluded the possibility of systematic errors due to pressure shift, and we have confirmed the accuracy of our frequency comb calibration within tens of kHz using a known transition of methane. Most importantly, the independent measurement of the same CH$_5^+$ transition by Schlemmer's group[38] is the strongest evidence that our technique does not exhibit errors of order 5 MHz, which provides us with the utmost confidence in the values that we have reported.

The instrument is currently limited in wavelength coverage by the coverage of our OPO module (3.2–3.9 μm), and to some extent by the coatings of our external cavity mirrors (nominally 3.0–3.4 μm, but usable outside this range). However, OPO modules are available that cover 2.3–4.6 μm, and it should be possible to produce moderate reflectivity (∼99.0–99.7%) cavity mirrors across that range. Considering the chemical versatility of the positive column discharge and the general applicability of direct absorption/dispersion spectroscopy, our technique will enable the high-precision,

high-accuracy spectroscopy of a wide variety of molecular ions. Possible applications include tests of high accuracy *ab initio* calculations, supporting astronomical observations, and aiding in the assignment of congested spectra.

[1] C. Gudeman, M. Begemann, J. Pfaff, and R. Saykally, Phys. Rev. Lett. **50**, 727 (1983).

[2] S. K. Stephenson and R. J. Saykally, Chem. Rev. **105**, 3220 (2005).

[3] E. T. White, J. Tang, and T. Oka, Science **284**, 135 (1999).

[4] T. Amano, J. Chem. Phys. **79**, 3595 (1983).

[5] A. A. Mills, B. M. Siller, and B. J. McCall, Chem. Phys. Lett. **501**, 1 (2010).

[6] B. M. Siller, A. A. Mills, and B. J. McCall, Opt. Lett. **35**, 1266 (2010).

[7] B. M. Siller, M. W. Porambo, A. A. Mills, and B. J. McCall, Opt. Express **19**, 24822 (2011).

[8] L.-S. Ma, J. Ye, P. Dubé, and J. L. Hall, J. Opt. Soc. Am. B **16**, 2255 (1999).

[9] K. N. Crabtree, J. N. Hodges, B. M. Siller, A. J. Perry, J. E. Kelly, P. A. Jenkins, and B. J. McCall, Chem. Phys. Lett. **551**, 1 (2012).

[10] B. M. Siller, J. N. Hodges, A. J. Perry, and B. J. McCall, "Indirect rotational spectroscopy of HCO$^+$," J. Phys. Chem. A **117**(39), 10034–10040 (2013).

[11] M. Pavanello, L. Adamowicz, A. Alijah, N. F. Zobov, I. I. Mizus, O. L. Polyansky, J. Tennyson, T. Szidarovszky, A. G. Császár, M. Berg, A. Petrignani, and A. Wolf, Phys. Rev. Lett. **108**, 023002 (2012).

[12] J. Komasa, K. Piszczatowski, G. Łach, M. Przybytek, B. Jeziorski, and K. Pachucki, J. Chem. Theory Comput. **7**, 3105 (2011).

[13] P. Pyykkö, K. Dyall, A. Császár, G. Tarczay, O. Polyansky, and J. Tennyson, Phys. Rev. A **63**, 024502 (2001).

[14] T. R. Geballe and T. Oka, Nature **384**, 334 (1996).

[15] N. Indriolo and B. J. McCall, Astrophys. J. **745**, 91 (2012).

[16] P. Drossart, J.-P. Maillard, J. Caldwell, S. J. Kim, J. K. G. Watson, W. A. Majewski, J. Tennyson, S. Miller, S. K. Atreya, J. T. Clarke, J. H. Waite, and R. Wagener, Nature **340**, 539 (1989).

[17] D. Rego, N. Achilleos, T. Stallard, and S. Miller, Nature **399**, 121 (1999).

[18] C. Savage, F. Dong, and D. J. Nesbitt, in *60th International Symposium on Molecular Spectroscopy, Talk MG06* (2005).

[19] K.-Y. Wu, "Precision Measurement of the ν_2-band of triatomic hydrogen molecular ion H$_3^+$," Ph.D. thesis, National Tsing Hua University, 2008.

[20] A. McKellar and J. Watson, J. Mol. Spectrosc. **191**, 215 (1998).

[21] T. Oka, Philos. Trans. R. Soc. London, Ser. A **303**, 543 (1981).

[22] H.-C. Chen, C.-Y. Hsiao, J.-L. Peng, T. Amano, and J.-T. Shy, Phys. Rev. Lett. **109**, 263002 (2012).

[23] H.-C. Chen, J.-L. Peng, T. Amano, and J.-T. Shy, in *68th International Symposium on Molecular Spectroscopy, Talk MG05* (2013).

[24] K. Takahata, T. Kobayashi, H. Sasada, Y. Nakajima, H. Inaba, and F.-L. Hong, Phys. Rev. A **80**, 032518 (2009).

[25] A. Foltynowicz, W. Ma, and O. Axner, Opt. Express **16**, 14689 (2008).

[26] A. Foltynowicz, I. Silander, and O. Axner, J. Opt. Soc. Am. B **28**, 2797 (2011).

[27] J. Westberg, P. Kluczynski, S. Lundqvist, and O. Axner, J. Quant. Spectrosc. Radiat. Transf. **112**, 1443 (2011).

[28] G. Cazzoli, L. Cludi, G. Buffa, and C. Puzzarini, Astrophys. J., Suppl. Ser. **203**, 11 (2012).

[29] P. R. Bunker, B. Ostojić, and S. Yurchenko, J. Mol. Struct. **695–696**, 253 (2004).

[30] Z. Jin, B. J. Braams, and J. M. Bowman, J. Phys. Chem. A **110**, 1569 (2006).

[31] X. Huang, A. B. McCoy, J. M. Bowman, L. M. Johnson, C. Savage, F. Dong, and D. J. Nesbitt, Science **311**, 60 (2006).

[32] M. P. Deskevich, A. B. McCoy, J. M. Hutson, and D. J. Nesbitt, J. Chem. Phys. **128**, 094306 (2008).

[33] C. E. Hinkle and A. B. McCoy, J. Phys. Chem. A **112**, 2058 (2008).

[34] X.-G. Wang and T. Carrington, Jr., J. Chem. Phys. **129**, 234102 (2008).

[35] C. E. Hinkle, A. S. Petit, and A. B. McCoy, J. Mol. Spectrosc. **268**, 189 (2011).

[36] O. Asvany, P. Kumar, B. Redlich, I. Hegemann, S. Schlemmer, and D. Marx, Science **309**, 1219 (2005).

[37] O. Asvany, J. Krieg, and S. Schlemmer, Rev. Sci. Instrum. **83**, 093110 (2012).

[38] S. Schlemmer, private communication (2013).

[39] J. M. L. Martin, P. R. Taylor, and T. J. Lee, J. Chem. Phys. **99**, 286 (1993).

Communication: High precision sub-Doppler infrared spectroscopy of the HeH+ ion

Adam J. Perry, James N. Hodges, Charles R. Markus, G. Stephen Kocheril, and Benjamin J. McCall

Articles you may be interested in

Communication: He-tagged vibrational spectra of the SarGlyH+ and H+(H2O)2,3 ions: Quantifying tag effects in cryogenic ion vibrational predissociation (CIVP) spectroscopy
J. Chem. Phys. **140**, 221101 (2014); 10.1063/1.4880475

Properties of the B+-H2 and B+-D2 complexes: A theoretical and spectroscopic study
J. Chem. Phys. **137**, 124312 (2012); 10.1063/1.4754131

Rotationally resolved infrared spectrum of the Na+-D2 complex: An experimental and theoretical study
J. Chem. Phys. **134**, 214302 (2011); 10.1063/1.3596720

A three-dimensional ab initio potential energy surface and predicted infrared spectra for the He – N 2 O complex
J. Chem. Phys. **124**, 144317 (2006); 10.1063/1.2189227

Infrared laser absorption spectroscopy of rotational and vibration rotational transitions of HeH + up to the dissociation threshold
J. Chem. Phys. **107**, 337 (1997); 10.1063/1.474394

Communication: High precision sub-Doppler infrared spectroscopy of the HeH+ ion

Adam J. Perry,[1] James N. Hodges,[1] Charles R. Markus,[1] G. Stephen Kocheril,[1] and Benjamin J. McCall[1,2,a]

[1]*Department of Chemistry, University of Illinois, Urbana, Illinois 61801, USA*
[2]*Departments of Astronomy and Physics, University of Illinois, Urbana, Illinois 61801, USA*

The hydrohelium cation, HeH+, serves as an important benchmark for *ab initio* calculations that take into account non-adiabatic, relativistic, and quantum electrodynamic effects. Such calculations are capable of predicting molecular transitions to an accuracy of ∼300 MHz or less. However, in order to continue to push the boundaries on these calculations, new measurements of these transitions are required. Here we measure seven rovibrational transitions in the fundamental vibrational band to a precision of ∼1 MHz using the technique of Noise Immune Cavity Enhanced Optical Heterodyne Velocity Modulation Spectroscopy. These newly measured transitions are included in a fit to the rotation-vibration term values to derive refined spectroscopic constants in the v = 0 and v = 1 vibrational states, as well as to calculate rotation-vibration energy levels with high precision. © 2014 AIP Publishing LLC. [http://dx.doi.org/10.1063/1.4895505]

I. INTRODUCTION

Composed of the two most abundant elements in the universe, the HeH+ cation is predicted to be among the first molecules ever formed,[1,2] which makes this species of vital significance to chemical models of the early universe. Astronomical observations targeted at HeH+ have yet to yield an unequivocal detection of this molecule. The difficulty in detecting this species is attributed to the many chemical processes that compete with the formation of HeH+, ultimately resulting in a low abundance of this molecule. However, this molecule is easily formed in laboratory plasmas, which has spurred much experimental work on this fundamental species.

First discovered in 1925,[3] the HeH+ ion has been the subject of many spectroscopic studies. In 1979, the first rovibrational spectrum of this molecule was acquired by Tolliver and co-workers, who observed the P(12) and P(13) lines in the fundamental vibrational band as well as the P(9)-P(11) transitions in the v = 2 ← 1 hot band with an accuracy of ∼0.002 cm^{-1}.[4] In 1982, Bernath and Amano reported the first observation of the low J transitions in the fundamental band, covering the P(4)-R(4) rovibrational transitions.[5] After this work various studies of hot bands were published, including transitions from bound to quasibound states as well as quasibound to quasibound transitions.[6–8] In 1989, Crofton and co-workers measured a few new transitions in the fundamental band along with several lines in the v = 2 ← 1 hot band as well as in the fundamental bands of the ^{3}HeH+, ^{4}HeD+, and ^{3}HeD+ isotopologues.[9] Pure rotational studies were first carried out by Liu *et al.* where the J = 7 ← 6 transition was measured,[10] followed by the measurement of J = 1 ← 0 and J = 2 ← 1 by Matsushima *et al.*[11] as well as some low J

rotational transitions of the ^{3}HeH+, ^{4}HeD+, and ^{3}HeD+ isotopologues. Higher J rotational transitions were measured by Liu and Davies[8,12] with J as high as 25.

From a theoretical standpoint the HeH+ ion is a relatively simple species that is isoelectronic to H$_2$. This makes HeH+ an important benchmark molecule for high-level *ab initio* calculations that take into account not only non-adiabatic corrections to the Born Oppenheimer approximation, but also relativistic and quantum electrodynamic (QED) effects. Recent *ab initio* calculations by Pachucki and Kosama,[13] which have treated the non-adiabatic corrections using Non-Adiabatic Perturbation Theory as well as the relativistic (α^2) and leading QED (α^3) corrections to the Born-Oppenheimer approximation, have been able to reproduce many experimentally measured rovibrational transitions with an accuracy on the order of 0.01 cm^{-1}(∼300 MHz). This sort of accuracy is only currently achievable for a select few molecular systems, namely, H$_2$, H$_2^+$, H$_3^+$, and HeH+.[13–17] In order to predict transition frequencies with accuracies on the level of 0.001 cm^{-1}or better for more complicated systems, it is imperative that the theoretical treatment of the aforementioned benchmark systems be well developed. Since theory must be informed by experiment to push the boundaries of these calculations, experimentalists need to provide highly accurate and precise measurements of molecular transitions for these species.

The HeH+ molecule has also proven to be a useful benchmark system for theoretical treatments that go beyond the Born-Oppenheimer approximation.[18] These methods rely on using a set of correlated Gaussian functions that are functions of the separations between the nuclei and electrons, thus eliminating the traditional separation of the nuclear and electronic wavefunctions of the Born-Oppenheimer approximation. Within this framework the authors also developed algorithms for calculating the complete relativistic correction for this molecule.[19,20] To date, these sorts of calculations have

---

a)Electronic mail: bjmccall@illinois.edu

only been performed on states with no angular momentum (i.e., "rotationless" states).

Another approach has been to develop a global empirical potential that is based on the available spectroscopic data.[21] This work used all available spectroscopic data from all isotopomers in a fit to a modified Lennard-Jones potential that is able to provide the correct behavior at large internuclear separations near the dissociation limit. This approach also allows for experimental determination of the Born-Oppenheimer breakdown functions which showed reasonable agreement with a fitted theoretical potential based on the calculations of Bishop and Cheung.[22]

II. EXPERIMENTAL

The instrument used in this work has been described in detail in Ref. 23 and therefore will be described here only briefly. For this work, we used a technique that has been previously developed in our lab called Noise Immune Cavity Enhanced Optical Heterodyne Velocity Modulation Spectroscopy (NICE-OHVMS)[23–25] which combines the high sensitivity of Noise Immune Cavity Enhanced Optical Heterodyne Molecular Spectroscopy (NICE-OHMS)[26] with the ion/neutral discrimination of velocity modulation spectroscopy.[27]

The spectrometer is based on a commercially available continuous wave optical parametric oscillator (Aculight Argos 2400 SF) that is tunable across the 3.2–3.9 μm range. The pump laser (Koheras Adjustik Y-10) is phase modulated at a frequency of ~80 MHz to produce a pair of RF sidebands that are imprinted onto the idler wave. The idler wave is then coupled into an external optical cavity (finesse of ~150) which surrounds a liquid nitrogen cooled positive column discharge cell, in which ions of interest are produced from precursor gasses (a 2 Torr mixture of H_2 and He in a 1:100 ratio) and where their absorption profiles are velocity modulated. Light transmitted through the cavity is detected by a fast photodiode detector (Boston Electronics Vigo PVM-10.6-1×1), from which the signal is demodulated at the same frequency used

to generate the 80 MHz sidebands, using a pair of frequency mixers that are 90° out of phase with one another. Further demodulation of the mixer outputs at twice the velocity modulation frequency (~80 kHz) is accomplished by a pair of lock-in amplifiers, which acts to recover the velocity modulation information.

Frequency calibration of our spectra was accomplished using an optical frequency comb (Menlo Systems FC-1500 with 100 MHz repetition rate) to measure the difference in frequency of the pump and signal beams at each point. Initial measurements of the frequencies of both beams (ten measurements for each) are performed using a near-infrared wavemeter (Burleigh WA-1500) to determine the mode number of the nearest comb tooth. The accuracy of the wavemeter was enhanced by measuring nearby reference lines of CH_4.[28] These reference line frequencies are all determined to within ~5 MHz and any systematic errors introduced by the wavemeter can be corrected to ensure that the proper comb mode numbers are determined.

III. RESULTS

Figure 1 shows a typical NICE-OHVMS spectrum of the P(1) transition of HeH^+ at 85258146.86(35) MHz. The lineshapes have an odd symmetry resulting from the heterodyne detection and velocity modulation schemes. The narrow features near the center of the lines are blends of several individual Lamb dips that are spaced by half-integer multiples of the heterodyne frequency about the center of the transition. To extract the transition line centers, we fit the data from all four of the detection channels simultaneously (Figure 2) with some shared parameters between the data channels such as the line center, full-width of the blended feature, and the heterodyne detection angle. Further information regarding the fitting routines has been given by Hodges *et al.*[23]

Table I shows that our measurements exhibit good agreement with the values measured by Bernath and Amano as all measured transitions lie within or only slightly outside their 30–60 MHz claimed uncertainties. However, in this work we
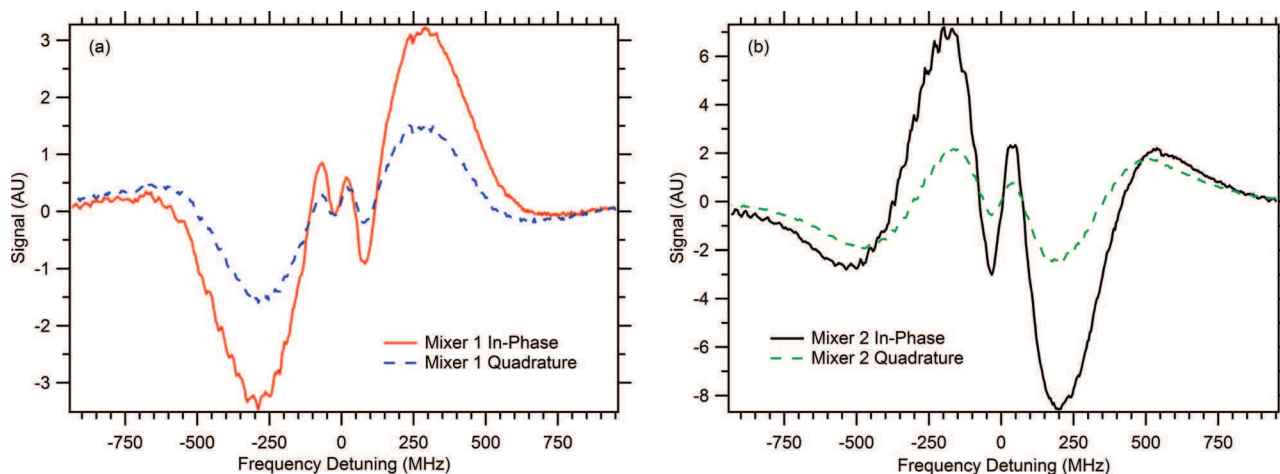

FIG. 1. Typical NICE-OHVMS scan of the P(1) fundamental band transition of HeH^+ showing the central Lamb dip feature sitting on top of the Doppler profile of the line. Signals from each of the four detection channels are shown with the in-phase (red solid trace) and quadrature (blue dashed trace) channels from mixer 1 plotted in panel (a) and the in-phase (black solid trace) and quadrature (green dashed trace) channels of mixer 2 in panel (b).
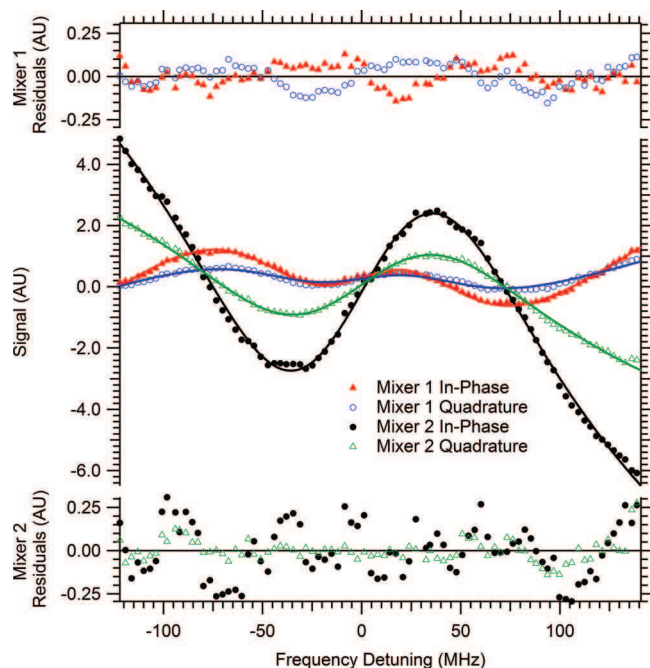
FIG. 2. Frequency comb calibrated scan of the central sub-Doppler Lamb dip feature in the P(1) rovibrational transition of HeH$^+$, along with a simultaneous fit of all four data acquisition channels. Colored markers represent the experimental data, while the colored solid traces show the fit of the data to the equation outlined in Hodges *et al.*[23] Fit residuals from each detection channel are plotted on the upper (channels from mixer 1) and lower (channels from mixer 2) axes. For clarity, only every third data point is shown.

have improved the precision on these measurements by two orders of magnitude. For all of the measurements we were able to obtain precisions on the order of 1 MHz for the line centers due to both our ability to saturate the transitions which allows us to fit the relatively narrow sub-Doppler features, and the frequency calibration provided by the optical frequency comb which allows us to go far beyond the typical tens of MHz measurement uncertainty provided by mid-infrared wavemeters and Doppler-broadened reference gas lines.

These new measurements together with all available data for the fundamental band[4,5,7,9] as well as pure rotational data[8,10,11] were included in a fit to a power-series expansion of the vibration-rotation term values for a $^1\Sigma$ linear molecule as shown in Eq. (1) [The measurements of P(9)-P(11) by Purder *et al.* were not included in the fit as no uncertainties were

TABLE I. All measured rovibrational transitions in the fundamental vibrational band of HeH$^+$ and a comparison to those values measured by Bernath and Amano.[5] All units are in MHz.

Transition	Freq.	St. Dev.	Prev. value[5]	Diff.
P(3)	80795499.88	0.99	80795566.39	− 66.51
P(2)	83096617.69	1.34	83096650.39	− 32.69
P(1)	85258146.86	0.35	85258082.06	64.80
R(0)	89115533.66	1.38	89115502.62	31.04
R(1)	90788380.66	0.40	90788398.50	− 17.84
R(2)	92275879.63	0.77	92275875.74	3.89
R(3)	93567523.38	0.92	93567519.55	3.82

TABLE II. Rovibrational parameters from a fit of experimentally measured rotation and rovibration transitions to Eq. (1). All units are in MHz.

Parameter	This work	Liu and Davies[8]
ν_0	87268330.62(54)	87268319(33)
B_0	1006063.39(15)	1006063.3(45)
D_0	486.1762(187)	486.512(96)
H_0	0.1807358(2628)	0.18428(84)
$L_0 \times 10^4$	−1.17975(1418)	−1.331(36)
$M_0 \times 10^7$	0.73228(3114)	1.022(69)
$N_0 \times 10^{10}$	−0.49376(2392)	−0.702(48)
B_1	924550.54(17)	924554.8(45)
D_1	475.1636(138)	475.606(99)
H_1	0.1660888(3241)	0.17049(84)
$L_1 \times 10^4$	−1.31950(2056)	−1.499(33)
$M_1 \times 10^7$	1.05510(4957)	1.385(60)
$N_1 \times 10^{10}$	−1.12488(4121)	−1.352(42)

reported],[29]

$$F_v = G_v + B_v J(J+1) - D_v[J(J+1)]^2 + H_v[J(J+1)]^3$$

$$+L_v[J(J+1)]^4 + M_v[J(J+1)]^5 + N_v[J(J+1)]^6.$$
(1)

The fit was performed using PGOPHER,[30] floating all parameters in both the ground and first excited vibrational states. In addition to our high-precision rovibrational measurements and the remaining fundamental band data, the fit includes the two pure rotational transitions (J = 1 ← 0 and J = 2 ← 1) measured by Matsushima *et al.* with very high precision (∼200 kHz), as well as the pure rotational transitions of Liu and Davies, which includes 11 transitions in both the v = 0 and v = 1 vibrational states covering a range of J″ from 10 to 20. Parameters from the fit are given in Table II along with a comparison to those values obtained by Liu and Davies.[8] Full details of the fit can be found in the supplementary material.[31] Inclusion of these high precision measurements allows for a more precise determination (by roughly an order of magnitude) of the band origin as well as the B rotational constants and the lower order centrifugal distortion terms up to H.

It is interesting to note that for all the centrifugal distortion terms there are significant differences between our values and those of Liu and Davies. However, the results of the fit showed that the weighted residuals were randomly distributed across the entire range of J″, which suggests that the differences in the fit parameters may be due to a high degree of correlation among the higher order parameters. Indeed, when the correlation matrix is examined it is clear that this is the case as the H, L, M, and N parameters all show correlations of ≥ 0.9 with each other.

Another comparison can be made to the fit produced by Matsushima *et al.*[11] In their fit they only included their J = 1 ← 0 and J = 2 ← 1 transitions along with the available rovibrational data in the fundamental band, while only including terms up to L (the values of L were fixed to the *ab initio* predictions of Bishop and Cheung[22]). By doing so they were able to obtain very precise values for the B, D, and H values, which are nearly an order of magnitude more precise

TABLE III. Experimentally determined rotation-vibration energy levels $E(v,J)$ for $^4HeH^+$. All units are in MHz.

J	E(0,J)	E(1,J)
0	0	87268330.76(41)
1	2010183.86(20)	89115533.7(14)
2	6018916.87(28)	92798564.52(44)
3	12003064.7(11)	98294796.51(83)
4	19928164(60)	105570588.0(14)
5	29749118(30)	114581537(85)
6	41409933(172)	125273098(153)
7	54845432(194)	137580625(228)
8		151431127(245)

than the values reported in Table II. It may be the case, however, that the quality of their fit was somewhat fortuitous, due to the weighting of the highly precise values for the rotational transitions and their influence on the values of the lower order rotational parameters. We conjecture that since these lower order parameters were tightly constrained by only two transitions, their fit may have yielded well-determined parameters because there was so much more relative uncertainty in the rovibrational transition frequencies. The inclusion of our data, which also probe the J = 0, 1, and 2 levels in the ground vibrational state and carry a similar weighting in the fit as Matsushima's rotational transitions, may explain the apparent increase in the uncertainty of our parameters.

To further assess the accuracy of our measurements we performed a test by adding Gaussian noise of varying amounts (as determined by the standard deviation of this added noise) to our transition frequencies and running the fit described above using these modified frequencies. For noise with a standard deviation of 2 MHz we begin to see a noticeable degradation in the quality of the fit in terms of the residuals of our seven measured transitions. With this amount of "noise" we find that the RMS of the residuals for these seven transitions increases by roughly a factor of two. Though this test may not be 100% conclusive due to the random nature of adding in this noise, it does give us confidence that our claimed uncertainties are appropriate in size.

Using these new data along with previous infrared and pure rotational work, a set of experimentally determined rovibrational energy levels can be derived using a combination difference analysis. Evaluating the energy levels in this way is advantageous because they are not based on any model Hamiltonian. The energy levels covering J = 0–7 in the vibrational ground state and J = 0–8 in the v = 1 vibrational excited state can be computed based on the available spectroscopic data. Table III summarizes the results.

The high precision (no larger than 1.4 MHz) of the J = 3 level in the ground vibrational state and the first five rotational levels in the v = 1 vibrational state, will allow these energy levels to serve as excellent benchmark values for new *ab initio* calculations on this molecule.

IV. CONCLUSION

We have performed sub-Doppler mid-infrared spectroscopy on the HeH$^+$ cation. By using the technique of NICE-OHVMS in conjunction with frequency calibration provided by an optical frequency comb, we have re-measured seven fundamental band transitions of this molecule with a precision on the order of 1 MHz, and were able to achieve sub-MHz precision on most of the measured transitions. Using these new transitions with their improved uncertainties we have improved the values of the band origin as well as the B rotational constants and the lower order centrifugal distortion terms in a fit that includes all available spectroscopic data for the v = 0 and v = 1 states of the ^{4}HeH$^+$ molecule. These new measurements also allowed for very precise determination of the low J rotation-vibration energy levels in the ground and v = 1 states, which will serve as new benchmarks for theorists to test *ab initio* calculations as higher level non-adiabatic, relativistic, and QED corrections are included. These measurements could also be used in a refinement of the empirical potential originally published by Coxon and Hajigergiou.[21]

[1] S. Lepp, P. C. Stancil, and A. Dalgarno, J. Phys. B **35**, R57 (2002).
[2] S. Lepp, Astrophys. Space Sci. **285**, 737 (2003).
[3] T. R. Hogness and E. G. Lunn, Phys. Rev. **26**, 44 (1925).
[4] D. E. Tolliver, G. A. Kyrala, and W. H. Wing, Phys. Rev. Lett. **43**, 1719 (1979).
[5] P. Bernath and T. Amano, Phys. Rev. Lett. **48**, 20 (1982).
[6] A. Carrington, R. A. Kennedy, T. P. Softley, P. G. Fournier, and E. G. Richard, Chem. Phys. **81**, 251 (1983).
[7] C. E. Blom, K. Möller, and R. R. Filgueira, Chem. Phys. Lett. **140**, 489 (1987).
[8] Z. Liu and P. B. Davies, J. Chem. Phys. **107**, 337 (1997).
[9] M. W. Crofton, R. S. Altman, N. N. Haese, and T. Oka, J. Chem. Phys. **91**, 5882 (1989).
[10] D.-J. Liu, W.-C. Ho, and T. Oka, J. Chem. Phys. **87**, 2442 (1987).
[11] F. Matsushima, T. Oka, and K. Takagi, Phys. Rev. Lett. **78**, 1664 (1997).
[12] Z. Liu and P. B. Davies, Phys. Rev. Lett. **79**, 2779 (1997).
[13] K. Pachucki and J. Komasa, J. Chem. Phys. **137**, 204314 (2012).
[14] J. Komasa, K. Piszczatowski, G. Łach, M. Przybytek, B. Jeziorski, and K. Pachucki, J. Chem. Theory Comput. **7**, 3105 (2011).
[15] R. E. Moss, J. Phys. B **32**, L89 (1999).
[16] L. Lodi, O. L. Polyansky, J. Tennyson, A. Alijah, and N. F. Zobov, Phys. Rev. A **89**, 032505 (2014).
[17] W.-C. Tung, M. Pavanello, and L. Adamowicz, J. Chem. Phys. **137**, 164305 (2012).
[18] M. Stanke, D. Kędziera, M. Molski, S. Bubin, M. Barysz, and L. Adamowicz, Phys. Rev. Lett. **96**, 233002 (2006).
[19] S. Bubin, M. Stanke, D. Kędziera, and L. Adamowicz, Phys. Rev. A **76**, 022512 (2007).
[20] M. Stanke, D. Kędziera, S. Bubin, and L. Adamowicz, Phys. Rev. A **77**, 022506 (2008).
[21] J. A. Coxon and P. G. Hajigeorgiou, J. Mol. Spectrosc. **193**, 306 (1999).

[22]D. M. Bishop and L. M. Cheung, J. Mol. Spectrosc. **75**, 462 (1979).

[23]J. N. Hodges, A. J. Perry, P. A. Jenkins, B. M. Siller, and B. J. McCall, J. Chem. Phys. **139**, 164201 (2013).

[24]B. M. Siller, M. W. Porambo, A. A. Mills, and B. J. McCall, Opt. Exp. **19**, 24822 (2011).

[25]K. N. Crabtree, J. N. Hodges, B. M. Siller, A. J. Perry, J. E. Kelly, P. A. Jenkins, and B. J. McCall, Chem. Phys. Lett. **551**, 1 (2012).

[26]J. Ye, L.-S. Ma, and J. L. Hall, J. Opt. Soc. Am. B **15**, 6 (1998).

[27]C. S. Gudeman, M. H. Begemann, J. Pfaff, and R. J. Saykally, Phys. Rev. Lett. **50**, 727 (1983).

[28]L. S. Rothman, I. E. Gordon, Y. Babikov, A. Barbe, D. Chris Benner, P. F. Bernath, M. Birk, L. Bizzocchi, V. Boudon, L. R. Brown, A. Campargue, K. Chance, E. A. Cohen, L. H. Coudert, V. M. Devi, B. J. Drouin, A. Fayt, J.-M. Flaud, R. R. Gamache, J. J. Harrison, J.-M. Hartmann, C. Hill, J. T. Hodges, D. Jacquemart, A. Jolly, J. Lamouroux, R. J. Le Roy, G. Li, D. A. Long, O. M. Lyulin, C. J. Mackie, S. T. Massie, S. Mikhailenko, H. S. P. Müller, O. V. Naumenko, A. V. Nikitin, J. Orphal, V. Perevalov, A. Perrin, E. R. Polovtseva, C. Richard, M. A. H. Smith, E. Starikova, K. Sung, S. Tashkun, J. Tennyson, G. C. Toon, Vl. G. Tyuterev, and G. Wagner, J. Quant. Spectrosc. Radiat. Transf. **130**, 4 (2013).

[29]J. Purder, S. Civiš, C. E. Blom, and M. C. van Hemert, J. Mol. Spectrosc. **153**, 701 (1992).

[30]C. M. Western, PGOPHER, a Program for Simulating Rotational Structure, University of Bristol, http://pgopher.chm.bris.ac.uk.

[31]See supplementary material at http://dx.doi.org/10.1063/1.4895505 for the fit details of each experimentally measured transition.